ISSN : 2165-4069(Online)
ISSN : 2165-4050(Print)

IJARAI

International Journal of
Advanced Research in Artificial Intelligence

Volume 1 Issue 6

www.ijarai.thesai.org

A Publication of
The Science and Information Organization

INTERNATIONAL JOURNAL OF ADVANCED RESEARCH IN ARTIFICIAL INTELLIGENCE

THE SCIENCE AND INFORMATION ORGANIZATION

www.thesai.org | info@thesai.org












Editorial Preface

From the Desk of Managing Editor…

"The question of whether computers can think is like the question of whether submarines can swim." — Edsger W. Dijkstra, the quote explains the power of Artificial Intelligence in computers with the changing landscape. The renaissance stimulated by the field of Artificial Intelligence is generating multiple formats and channels of creativity and innovation.

This journal is a special track on Artificial Intelligence by The Science and Information Organization and aims to be a leading forum for engineers, researchers and practitioners throughout the world.

The journal reports results achieved; proposals for new ways of looking at AI problems and include demonstrations of effectiveness. Papers describing existing technologies or algorithms integrating multiple systems are welcomed. IJARAI also invites papers on real life applications, which should describe the current scenarios, proposed solution, emphasize its novelty, and present an in-depth evaluation of the AI techniques being exploited. IJARAI focusses on quality and relevance in its publications.

In addition, IJARAI recognizes the importance of international influences on Artificial Intelligence and seeks international input in all aspects of the journal, including content, authorship of papers, readership, paper reviewers, and Editorial Board membership.

The success of authors and the journal is interdependent. While the Journal is in its initial phase, it is not only the Editor whose work is crucial to producing the journal. The editorial board members , the peer reviewers, scholars around the world who assess submissions, students, and institutions who generously give their expertise in factors small and large— their constant encouragement has helped a lot in the progress of the journal and shall help in future to earn credibility amongst all the reader members.

I add a personal thanks to the whole team that has catalysed so much, and I wish everyone who has been connected with the Journal the very best for the future.

Thank you for Sharing Wisdom!

Managing Editor
IJARAI
Volume 1 Issue 5 August 2012
ISSN: 2165-4069(Online)
ISSN: 2165-4050(Print)

Editorial Board

Reviewer Board Members

CONTENTS

Human Gait Gender Classification in Spatial and Temporal Reasoning

Kohei Arai [1]
Graduate School of Science and Engineering
Saga University
Saga City, Japan

Rosa Andrie Asmara[2]
Graduate School of Science and Engineering
Saga University
Saga City, Japan

***Abstract*— Biometrics technology already becomes one of many application needs for identification. Every organ in the human body might be used as an identification unit because they tend to be unique characteristics. Many researchers had their focus on human organ biometrics physical characteristics such as fingerprint, human face, palm print, eye iris, DNA, and even behavioral characteristics such as a way of talk, voice and gait walking. Human Gait as the recognition object is the famous biometrics system recently. One of the important advantage in this recognition compare to other is it does not require observed subject's attention and assistance. This paper proposed Gender classification using Human Gait video data. There are many human gait datasets created within the last 10 years. Some databases that widely used are University of South Florida (USF) Gait Dataset, Chinese Academy of Sciences (CASIA) Gait Dataset, and Southampton University (SOTON) Gait Dataset. This paper classifies human gender in Spatial Temporal reasoning using CASIA Gait Database. Using Support Vector Machine as a Classifier, the classification result is 97.63% accuracy.**

Keywords- Gait Gender Classification; Gait Energy Motion; CASIA Gait Dataset.

I. INTRODUCTION

In recent years, there has been an increased attention on effectively identifying individuals for prevention of terrorist attacks. Many biometric technologies have emerged for identifying and verifying individuals by analyzing face, fingerprint, palm print, iris, gait or a combination of these traits [1][10][21].

Human Gait as the classification and recognition object is the famous biometrics system recently. Many researchers had focused this issue to consider for a new recognition system [2][3][4][5][11][14][17][18][19][20] [21][24].

Human Gait classification and recognition giving some advantage compared to other recognition system. Gait classification system does not require observed subject's attention and assistance. It can also capture gait at a far distance without requiring physical information from subjects [3][4][5].

There is a significant difference between human gait and other biometrics classification. In human gait, we should use video data instead of using image data as other biometrics system used widely. In video data, we can utilize spatial data as well as temporal data compare to image data. Most of the gait classification and or recognition system created are using spatial data only[2][3][4][5][11][14][17][18][19][20][21][24].

Human Gait Gender Classification as a recognition system divided in three main subject; preprocessing, feature extraction and classification.

There are 2 feature extraction method to be used: model based and free model approach [2][20]. We used free model-based for spatial data extraction and model-based for temporal data extraction. Model-based approaches obtain a set of static or dynamic skeleton parameters via modeling or tracking body components such as limbs, legs, arms and thighs. Gait signatures derived from these model parameters employed for identification and recognition of an individual. It is obvious that model-based approaches are view-invariant and scale-independent. These advantages are significant for practical applications, because it is unlikely that reference sequences and test sequences taken from the same viewpoint. Model-free approaches focus on shapes of silhouettes or the entire movement of physical bodies. Model-free approaches are insensitive to the quality of silhouettes. Its advantage is a low computational costs comparing to model-based approaches. However, they are usually not robust to viewpoints and scale [3].

There are some Human Gait Datasets widely used by researchers today. Many human gait datasets created within the last 10 years. Some of widely used datasets are University of South Florida (USF) Gait Dataset, Chinese Academy of Sciences (CASIA) Gait Dataset, and Southampton University (SOTON) Gait Dataset. Our proposed method uses CASIA as a dataset resource. We used Class B of CASIA Dataset.

CASIA Class B is a large multi-view gait database, created in January 2005. There are 124 subjects, and the gait was captured from 11 views.

This paper will presents the classification of Human gait gender classification using our proposed method, Gait Energy Motion as a spatial feature and movement velocity as a temporal feature. The following section describes the proposed gender classification based on human gait followed by implementation and some experiments. Then conclusion with some discussions is also followed.

II. PROPOSED METHOD

The classification of human gait in this paper consists of three part, preprocessing, feature extraction, and classification.

Figure 1 shows the complete overview of proposed human gait gender classification.

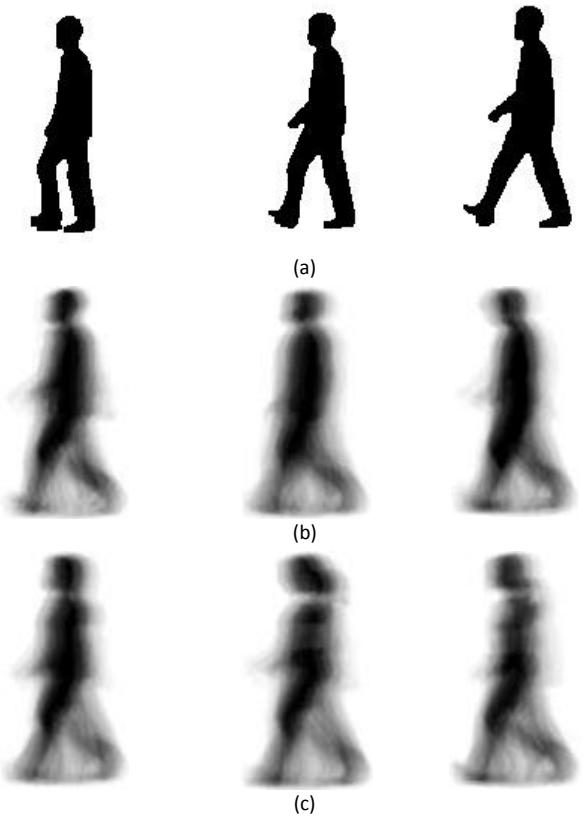

Figure 1(a). Silhouettes image (b). Male GEI image sample (c). Female GEI image sample

A. *Preprocessing*

In this proposed method, we use CASIA (Chinese Academy of Science) Gait Dataset of Class B using one perpendicular camera. The Class B Dataset consists of 124 different person. Each person had some conditions: bring bag, using coat, and normal condition. Each condition also taken some different angle camera position. The video resolution is 320 by 240 pixels, and using 25 fps of frame rate. We use a normal condition and perpendicular camera position. First step preprocessing to get the feature is creating silhouettes, fortunately we did not have to create silhouettes because CASIA also provide silhouettes image in their dataset. Usually, silhouettes created using background subtraction.

B. *Feature Extraction*

We used free model-based for spatial data extraction and model-based for temporal data extraction.

Free Model Based

Free Model based using Gait Energy Image (GEI) is the best feature for gait recognition and classification until now[2][20]. GEI have some advantage compare to other feature. GEI represents all the silhouettes in one video file, into one new energy image. The dimensionality of the data is reduced using the energy. Using GEI will also remove the noise smoothly. It is said that GEI is a spatial temporal data, but in fact there are no temporal information in GEI. To overcome the temporal data, we use the model based which will be discuss in the next section.

Using GEI for gender classification also already published [20]. Instead of using raw GEI, Shiqi Yu et al. used some weighting point in some parts of the human body. The weighting factor achieved from some survey that their team taken in the research. The accuracy for gait gender classification using GEI and weighting point by Shiqi Yu et al. is 95.97%.

Gender classification using gait motion as a feature also already done [26]. The gender classification accuracy is 92.9% using the gait motion.

To make comparative study with GEI, we will exploits motion feature as spatial data from human gait. Using the same method with GEI, but we just use the motion as a feature. We call this method Gait Energy Motion (GEM).

GEI is defined as [20] :

$$F(i,j) = \frac{1}{T}\sum_{t=1}^{T} I(i,j,t) \qquad (1)$$

where T is the number of frames in the sequence *I(i,j,.)*, *I(i,j,t)* is a binary silhouette image at frame *t*, *i*, and *j* are the image coordinates.

GEM is defined as :

$$F(i,j) = \frac{1}{T}\sum_{t=2}^{T} |I(i,j,t) - I(i,j,t-1)| \qquad (2)$$

where *I(i,j,t)* is a binary silhouette image at current frame *t*, and *I(i,j,t-1)* is a binary silhouette image at previous frame *t*. Figure 2 shows the flowchart for generating GEM.

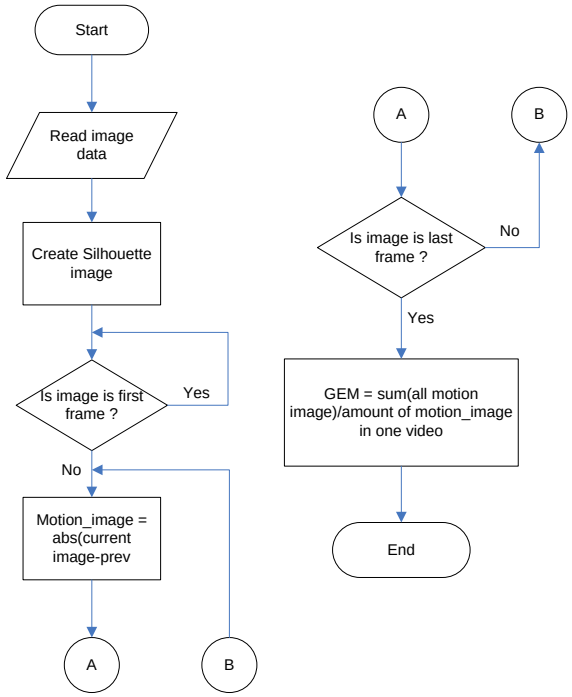

Figure 2. Flowchart for generating GEM

The model free preprocessing used in this paper by using the motion parameter per frame [22]. First, we have to get the silhouettes image. After we get the silhouettes, the motion of the human body can be achieved by using background

subtraction. The motion we get also per frame and per video sequence. Figure 3 (a) is the results of the silhouettes image. Figure 3 (b) is the example of the human motion per frame. Figure 3 (c) is the example of Gait Energy Motion.

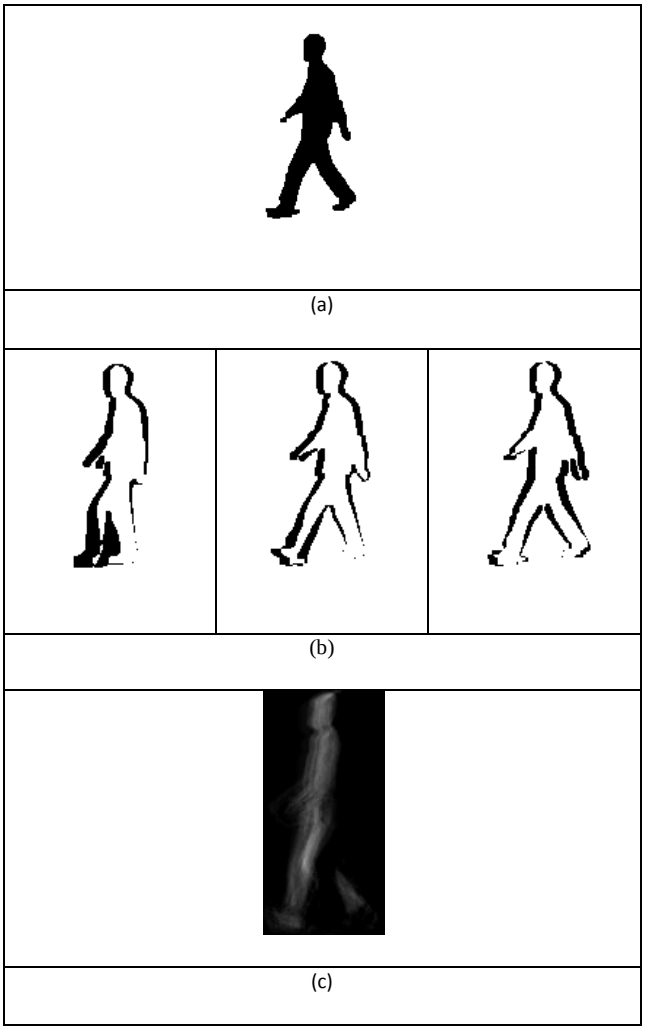

Figure 3. (a) Silhouettes image, (b) Motion image per frame, (c) Gait Energy Motion (GEM) result per video sequence.

Model based approaches obtain a series of static or dynamic body parameters via modelling or tracking body components such as limbs, legs, arms and thigh [2]. Model based approaches are view invariant and scale independent. Model based approaches are sensitive to the quality of gait sequences. Another disadvantage of the model based is its large computation and relatively high time costs due to parameters calculations.

Many gait model already made so far. We use M. S. Nixon et al. [4] model as a reference. This model provides more kinematics feature compare to other model. The challenge to this model is how to distinguish between left and right leg, because the data source only two-dimensional image using one perpendicular camera. This model can provide a lot of features, however, for the proposed method we start by only use one feature which is the velocity as a temporal data.

The methods namely Skeleton model. Morphological operation provides such a method to get skeleton image. The skeleton image having a lot of noise that can reduce the feature calculation result. For this research, we do not remove the noise because the we only used one temporal feature which is velocity.

We use three binary morphological operations to create such a skeleton model. Those three models are dilation, erosion, and thinning. For the dilation, we use three times of one's structuring element. We use six times of one's structuring element for the erosion.

Below is the algorithm for thinning operation [29]:

1. Divide the image into two distinct subfields in a checkerboard pattern.
2. In the first sub iteration, delete pixel *p* from the first subfield if and only if the conditions G_1, G_2, and G_3 are all satisfied.
3. In the second sub iteration, delete pixel *p* from the second subfield if and only if the conditions G_1, G_2, and G_3' are all satisfied.

Condition G_1: $X_H(p) = 1$ (3)

where :

$$X_H(p) = \sum_{i=1}^{4} b_i$$

$$b_i = \begin{cases} 1 \text{ if } x_{2i-1}=0 \text{ and } (x_{2i} = 1 \text{ or } x_{2i+1} = 1) \\ 0 \text{ otherwise} \end{cases}$$

Condition G_2: $2 \leq \min\{n_1(p), n_2(p)\} \leq 3$ (4)

where :

$$n_1(p) = \sum_{k=1}^{4} x_{2k-1} \vee x_{2k}$$

$$n_2(p) = \sum_{k=1}^{4} x_{2k} \vee x_{2k+1}$$

Condition G3: $(x_2 \vee x_3 \vee \overline{x_8}) \wedge x_1 = 0$ (5)

Condition G3': $(x_6 \vee x_7 \vee \overline{x_4}) \wedge x_5 = 0$ (6)

Figure 4 shows the result of silhouettes after some morphological operation proposed.

We can calculate the velocity easily using head point in every frame as a reference. The unit measure for velocity in this method is pixel/frame.

III. Implementation and Experiments

We will implement the proposed methods to the CASIA (Chinese Academy of Sciences) Gait Database. CASIA Gait dataset has four class datasets: Dataset A, Dataset B (multi-view dataset), Dataset C (infrared dataset), and Dataset D (foot pressure measurement dataset). We will use the B class dataset

in 90 degrees point of view. Figure 8 shows the CASIA Gait image database example of male and female gender [9].

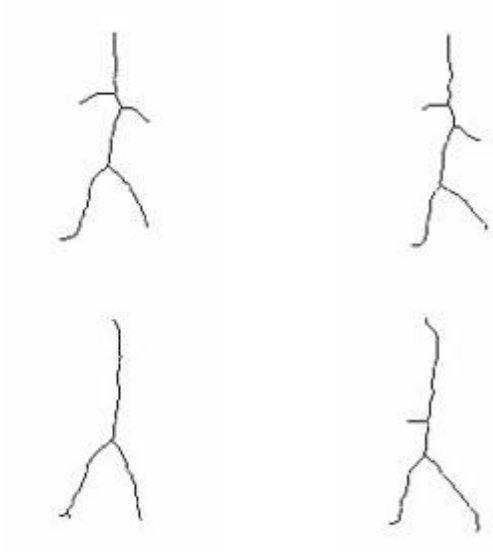

Figure 4. Skeleton after some morphological operation

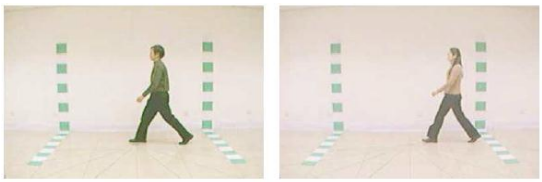

Figure 5. CASIA Gait image example of male and female

There are 124 unique human gaits in B class dataset. From the total of 124 dataset, only 31 data of female gait existed. To make the data balance, we will also use 31 male gait dataset. Every human has 6 video of perpendicular view, so we pretend to use every single video as one data. The total of the data is 372, consists of 186 video of male gait and 186 video of female gait.

We use Support Vector Machine: SVM as a classification method and using 10 cross fold validation as a training method. We also try the well-known Two Dimensional: 2D Discrete Wavelet Transformation: DWT with Haar base function for analyzing and comparing the results [26]. The result is in Table 1. Very interesting to analyze is the classification time for every method. Every pixel is pretend to be the feature want to classify. The classification cost will be higher if the image size is bigger. GEM is smaller image compare to GEI, because GEM only took the motion part, not all part of the image. Using Approximation detail in DWT will reduce the classification cost because the image size is rescaling four times smaller in level 1. Smaller image size will also reduce the CCR.

Since we use Gait Energy Motion (GEM) which is taking the motion parameter in the image, the difference between classes should be the motion. Also another basic question is which part of the human body giving the significance difference between classes.

TABLE I. CCR TABLE FOR SOME METHODS ANALYZED

Method	Classification Time	CCR
Gait Energy Image (GEI) with some weighting factor [20]	1078.5 ms	95.97 %
Gait Energy Motion (GEM)	722.2 ms	97.47 %
GEM with Velocity	**744.5 ms**	**97.63 %**
2D DWT GEM Lv 1. Using Approximation Coefficient	566.1 ms	97.22 %
2D DWT GEM Lv 1. Using Approximation Coefficient with Velocity	630 ms	97.32 %

In [20], Shiqi Yu et al. used analysis of variance (ANOVA) F-statistics to analyze the gait difference between classes. We will use the same method to analyze GEM difference. The ANOVA F-statistic is a measure to evaluate different features discriminative capability. The greater the F-statistic values will give better discriminative capability. The F-statistic is calculated as follows [20]:

$$F = \frac{\frac{1}{c-1}\sum_{i=1}^{c} n_i(\bar{x}_i-\bar{x})^2}{\frac{1}{n-c}\sum_{i=1}^{c}\sum_{j=1}^{n_i}(x_{ij}-\bar{x}_i)^2} \quad (7)$$

where x_{ij} is the j^{th} sample of class i, c is the number of classes, n_i is the sample number of class i, $n = \sum_{i=1}^{c} n_i$, $\bar{x}_i$ is the mean of samples in class i, and $\bar{x}$ is the mean of $\bar{x}_i$. If we implement in our research, the formula above will become:

$$F = \frac{180((\text{mean}_{\text{gem\_male}}-\text{mean}_{\text{gem\_all}})^2+(\text{mean}_{\text{gem\_female}}-\text{mean}_{\text{gem\_all}}))^2}{\frac{1}{370}(\sum(\text{gem}_{\text{male(i,j)}}-\text{mean}_{\text{gem\_male}})^2+\sum(\text{gem}_{\text{female(i,j)}}-\text{mean}_{\text{gem\_female}})^2)} \quad (8)$$

The calculated F-statistic values are shown in Figure. Whiter color means better discriminative capability. The highest discriminative value is seen in the left foot motion. Right foot motion also seen some discriminative value, but because of the longer distance than the left foot, the value is not too high. Other areas that have higher discriminative value than others are the hand motion.

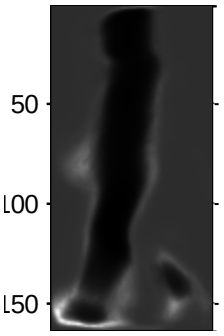

Figure 6. F-Statistics image

TABLE II. CCR FOR SOME PUBLISHED METHODS

Method	Dataset	CCR
Lee and Grimson	25 males & 25 females	85.0%
Huang and Wang [27]	25 males & 25 females	85.0%
Li et al. [19]	31 males & 31 females	93.28%
44 human observers	31 males & 31 females	95.47%
Shiqi Yu et al. [20]	31 males & 31 females	95.97%
Proposed method	31 males & 31 females	97.63%

VI. CONCLUSION

The entire system is using model free motion based and model motion based as spatial and temporal information. GEM as a spatial feature and velocity as a temporal feature extraction, and classify the data using SVM. Implemented in the CASIA Gait Database, we conclude as following:

(1) The classification accuracy is 97.47% if only spatial information processed.

(2) The classification accuracy is 97.63% if spatial and temporal information processed,

This research shows that GEM is giving more CCR result compare to GEI with some weighting factors. This research also shows that by using free model motion based and velocity gait is enough to use as a feature for human gait gender classification. We even do not need any weighting point factors in the feature to increase the classification result.

The preprocessing used in this proposed method is a model free based. There are some advantages by using this method. First, the development of the program is not difficult. Because it is not too difficult, another advantage of this method is low cost computation system.

We use velocity from a model based feature to get temporal information. This feature proved enough to classify gender. However, for human recognition using gait, we should use other kinematics parameter from a model that we created. There is some temporal information such as stride and cadence parameter per frame, angle of every knee per frame, and hip angle per frame. Some other classification might provide a better result to the recognition of human gait gender such as a k-nearest neighbor [14].

ACKNOWLEDGMENT

Portions of the research in this paper use the CASIA Gait Database collected by Institute of Automation, Chinese Academy of Sciences. In his connection, authors would like to thank to Chinese Academy of Sciences for their providing of the Gait database.

REFERENCES

[1] X. Qinghan, "Technology review – Biometrics Technology, Application, Challenge, and Computational Intelligence Solutions", IEEE Computational Intelligence Magazine, vol. 2, pp. 5-25, 2007.

[2] Jin Wang, Mary She, Saeid Nahavandi, Abbas Kouzani, "A Review of Vision-based Gait Recognition Methods for Human Identification", IEEE Computer Society, 2010 International Con-ference on Digital Image Computing: Techniques and Applications, pp. 320 - 327, 2010

[3] N. V. Boulgouris, D. Hatzinakos, and K. N. Plataniotis, "Gait recognition: a challenging signal processing technology for biometric identification", IEEE Signal Processing Magazine, vol. 22, pp. 78-90, 2005.

[4] M. S. Nixon and J. N. Carter, "Automatic Recognition by Gait", Proceedings of the IEEE, vol. 94, pp. 2013-2024, 2006.

[5] Y. Jang-Hee, H. Doosung, M. Ki-Young, and M. S. Nixon, "Automated Human Recognition by Gait using Neural Network", in First Workshops on Image Processing Theory, Tools and Applications, 2008, pp. 1-6.

[6] Wilfrid Taylor Dempster, George R. L. Gaughran, "Properties of Body Segments Based on Size and Weight", American Journal of Anatomy, Volume 120, Issue 1, pages 33–54, January 1967

[7] Gilbert Strang and Truong Nguen, "Wavelets and Filter Banks". Wellesley-Cambridge Press, MA, 1997, pp. 174-220, 365-382

[8] I. Daubechies, *Ten lectures on wavelets*, Philadelphis, PA : SIAM, 1992.

[9] CASIA Gait Database, http://www.cbsr.ia.ac.cn/ english/index.asp

[10] Edward WONG Kie Yih, G. Sainarayanan, Ali Chekima, "Palmprint Based Biometric System: A Comparative Study on Discrete Cosine Transform Energy, Wavelet Transform Energy and SobelCode Methods", Biomedical Soft Computing and Human Sciences, Vol.14, No.1, pp.11-19, 2009

[11] Dong Xu, Shuicheng Yan, Dacheng Tao, Stephen Lin, and Hong-Jiang Zhang, Marginal Fisher Analysis and Its Variants for Human Gait Recognition and Content- Based Image Retrieval, IEEE Transactions On Image Processing, Vol. 16, No. 11, November 2007

[12] Hui-Yu Huang, Shih-Hsu Chang, A lossless data hiding based on discrete Haar wavelet transform, 10th IEEE International Conference on Computer and Information Technology, 2010

[13] Kiyoharu Okagaki, Kenichi Takahashi, Hiroaki Ueda, Robustness Evaluation of Digital Watermarking Based on Discrete Wavelet Transform, Sixth International Conference on Intelligent Information Hiding and Multimedia Signal Processing, 2010

[14] Bogdan Pogorelc, Matjaž Gams, Medically Driven Data Mining Application: Recognition of Health Problems from Gait Patterns of Elderly, IEEE International Conference on Data Mining Workshops, 2010

[15] B.L. Gunjal, R.R.Manthalkar, Discrete Wavelet Transform based Strongly Robust Watermarking Scheme for Information Hiding in Digital Images, Third International Conference on Emerging Trends in Engineering and Technology, 2010

[16] Turghunjan Abdukirim, Koichi Niijima, Shigeru Takano, Design Of Biorthogonal Wavelet Filters Using Dyadic Lifting Scheme, Bulletin of Informatics and Cybernetics Research Association of Statistical Sciences, Vol.37, 2005

[17] Seungsuk Ha, Youngjoon Han, Hernsoo Hahn, Adaptive Gait Pattern Generation of Biped Robot based on Human's Gait Pattern Analysis, World Academy of Science, Engineering and Technology 34 2007

[18] Maodi Hu, Yunhong Wang, Zhaoxiang Zhang and Yiding Wang, Combining Spatial and Temporal Information for Gait Based Gender Classification, International Conference on Pattern Recognition 2010

[19] Xuelong Li, Stephen J. Maybank, Shuicheng Yan, Dacheng Tao, and Dong Xu, Gait Components and Their Application to Gender Recognition, IEEE Transactions On Systems, Man, And Cybernetics—Part C: Applications And Reviews, Vol. 38, No. 2, March 2008

[20] Shiqi Yu, , Tieniu Tan, Kaiqi Huang, Kui Jia, Xinyu Wu, A Study on Gait-Based Gender Classification, IEEE Transactions On Image Processing, Vol. 18, No. 8, August 2009

[21] M.Hanmandlu, R.Bhupesh Gupta, Farrukh Sayeed, A.Q.Ansari, An Experimental Study of different Features for Face Recognition, International Conference on Communication Systems and Network Technologies, 2011

[22] S. Handri, S. Nomura, K. Nakamura, Determination of Age and Gender Based on Features of Human Motion Using AdaBoost Algorithms, 2011

[23] Massimo Piccardi, Background Subtraction Techniques: Review, http://www-staff.it.uts.edu.au/ ~massimo/BackgroundSubtractionReview-Piccardi.pdf

[24] Rosa Asmara, Achmad Basuki, Kohei Arai, A Review of Chinese Academy of Sciences (CASIA) Gait Database As a Human Gait Recognition Dataset, published in the Industrial Electronics Seminar 2011, Surabaya Indonesia

[25] Bakshi, B., "Multiscale PCA with application to MSPC monitoring," AIChE J., 44, pp. 1596-1610., 1998
[26] Kohei Arai, Rosa Andrie, "Human Gait Gender Classification using 2D Discrete Wavelet Transforms Energy", IJCSNS International Journal of Computer Science and Network Security, Vol. 11 No. 12 pp. 62-68, December 2011
[27] G. Huang, Y. Wang, "Gender classification based on fusion of multi-view gait sequences," in Proc. 8th Asian Conf. Computer Vision, 2007, pp. 462-471.
[28] L. Lee, WEL Grimson, "Gait analysis for recognition and classification," in Proc. 5th IEEE Int. Conf. Automatic Face and Gesture Recognition, Washington, DC, May 2002, pp. 155-162.

AUTHORS PROFILE

Kohei Arai received BS, MS and PhD degrees in 1972, 1974 and 1982, respectively. He was with The Institute for Industrial Science and Technology of the University of Tokyo from April 1974 to December 1978 and also was with National Space Development Agency of Japan from January, 1979 to March, 1990. During from 1985 to 1987, he was with Canada Centre for Remote Sensing as a Post-Doctoral Fellow of National Science and Engineering Research Council of Canada. He moved to Saga University as a Professor in Department of Information Science on April 1990. He was a counselor for the Aeronautics and Space related to the Technology Committee of the Ministry of Science and Technology during from 1998 to 2000. He was a councilor of Saga University for 2002 and 2003. He also was an executive councilor for the Remote Sensing Society of Japan for 2003 to 2005. He is an Adjunct Professor of University of Arizona, USA since 1998. He also is Vice Chairman of the Commission A of ICSU/COSPAR since 2008. He wrote 29 books and published 352 journal papers.

Rosa A. Asmara received the B.E. degree in electronics engineering from Brawijaya University, and the M.S. degree in Multimedia engineering, from Institute of Technology Sepuluh Nopember, Surabaya, Indonesia, in 2004 and 2009, respectively. He is currently a PhD Student at Information Science in Saga University, Japan. His research interests include signal processing, image processing, parallel processing, pattern recognition, and computer vision

A Novel 9/7 Wavelet Filter banks For Texture Image Coding

Songjun Zhang [1]
School of Mathematics and Statistics
Xi'an Jiaotong University
Xi'an 710049, China

Guoan Yang [2]
School of electronics and informations
Xi'an Jiaotong University
Xi'an 710049, China

Zhengxing Cheng [3]
School of Mathematics and Statistics
Xi'an Jiaotong University
Xi'an 710049, China

Huub van de Wetering [4]
The Department of Mathematics and Computer Science
Technische Universiteit Eindhoven
Eindhoven, Holland

Xiaofeng Fang [5]
School of Mathematics and Statistics
Xi'an Jiaotong University
Xi'an 710049, China

***Abstract*— This paper proposes a novel 9/7 wavelet filter bank for texture image coding applications based on lifting a 5/3 filter to a 7/5 filter, and then to a 9/7 filter. Moreover, a one-dimensional optimization problem for the above 9/7 filter family is carried out according to the perfect reconstruction (PR) condition of wavelet transforms and wavelet properties. Finally, the optimal control parameter of the 9/7 filter family for image coding applications is determined by statistical analysis of compressibility tests applied on all the images in the Brodatz standard texture image database. Thus, a new 9/7 filter with only rational coefficients is determined. Compared to the design method of Cohen, Daubechies, and Feauveau, the design approach proposed in this paper is simpler and easier to implement. The experimental results show that the overall coding performances of the new 9/7 filter are superior to those of the CDF 9/7 filter banks in the JPEG2000 standard, with a maximum increase of 0.185315 dB at compression ratio 32:1. Therefore, this new 9/7 filter bank can be applied in image coding for texture images as the transform coding kernel.**

Keywords-9/7 wavelet filter banks; image coding; lifting scheme; texture image; Brodatz database.

I. INTRODUCTION

Wavelets can effectively be used in several domains including image segmentation, image enhancement, feature extraction, image retrieval, and image coding [1-3]. Although wavelets play an important role in the field of image coding, designing a wavelet kernel for a specific type of image coding, for instance texture images, is still problematic. The CDF 9/7 filter banks of the biorthogonal 9/7 wavelet proposed by Cohen, Daubechies, and Feauveau, is adopted by the JPEG2000 standard as a core algorithm. Although CDF 9/7 has had great impact and has a wide range of applications, its design method is too complicated and its VLSI hardware implementation is too complex. Therefore, this paper proposes new 9/7 filter banks based on Sweldens' lifting scheme [4-6]. Starting from the relatively simple 5/3 filter, this paper presents lifting to a 7/5 filter and subsequently to a 9/7 filter. Then, a one-dimensional parametric 9/7 filter family is derived, as well as providing the dynamic range of control parameters according to Daubechies regularity criterion. Finally, the 9/7 filter family designed in this paper is applied in an image coding application to Brodatz standard texture image database, where a new 9/7 filter bank with the optimal control parameter is determined by maximizing the PSNR (Peak Signal to Noise Ratio).

For the optimal design of biorthogonal wavelets, Cheng, constructed, based on the lifting algorithm, the compact support of biorthogonal wavelet filters and proposed a parametric expression for 9/7 wavelets [7]. In the meantime, Yang designed 9/7 and 7/5 wavelets on the basis of the lifting algorithm [8-9]. The lifting algorithm, presented in [7] and [9] adopts the Euclidean algorithm without providing the lifting operator that can directly improve to a 9/7 wavelet. Phoong and Vaidyanathan proposed the biorthogonal wavelet design method [10]. Antonini and Daubechies designed a wavelet base function for image compression through utilizing the visual features both in the space and frequency domain [11]. Wei and Burrus designed a novel compact support biorthogonal Coifman wavelet in the time domain [12]. The filter design methods mentioned in the above literature are based on traditional Fourier transform and do not use the lifting algorithm. To design a biorthogonal wavelet filter with vanishing moments of arbitrary multiplicity Liu proposed a method that solves trigonometric polynomial equations with two variables on the basis of Diophantine equations [13]. On the basis of filter optimization and median operation, Quan and Ho proposed an efficient lifting scheme to construct biorthogonal wavelet [14] with better compression

performance than the JPEG2000 standard CDF 9/7 wavelet; however, no optimal filter is provided in the literature for certain type of images. At present, there is relative little literature on texture image coding, yet the study of texture image coding is an important branch of image research, where Brodatz standard texture image database is one of the representative research subjects. The wavelet filter designed in this paper achieves better application performance in the coding of texture images.

This paper is organized as follows: Section 2 provides the basic theories of lifting scheme. Section 3 proposes a 9/7 wavelet filter design approach based on lifting scheme and the Euclidean algorithm and results in a one-dimensional parametric 9/7 wavelet filter. The range of the control variable of the one-dimensional parametric 9/7 wavelet filter designed in section 3 is determined in section 4. In section 5 this 9/7 wavelet filter is used for the coding of texture images in the Bordatz standard texture image database, an optimal parameter based on the PSNR criterion is determined, and, finally, experimental results for the optimized 9/7 wavelet filter bank are presented and analyzed. Section 5 states the conclusion of this paper and provides implications for future research.

II WAVELET LIFTING SCHEME

This paper focuses on biorthogonal wavelet filters. Let $\{h(z), g(z), \tilde{h}(z), \tilde{g}(z)\}$ be a compactly supported filter bank for such a wavelet. For filters $h(z)$ and $g(z)$, their polyphase representations are:

$$h(z) = h_e(z^2) + z^{-1}h_o(z^2)$$
$$g(z) = g_e(z^2) + z^{-1}g_o(z^2)$$

where

$$h_e(z) = \sum_k h_{2k} z^{-k}\ ,\ h_o(z) = \sum_k h_{2k+1} z^{-k}\ ,$$
$$g_e(z) = \sum_k g_{2k} z^{-k}\ ,\ g_o(z) = \sum_k g_{2k+1} z^{-k}\ .$$

And their polyphase matrix is:

$$P(z) = \begin{bmatrix} h_e(z) & g_e(z) \\ h_o(z) & g_o(z) \end{bmatrix} \quad (2)$$

Similarly, we can define a dual polyphase matrix $\tilde{P}(z)$:

$$\tilde{P}(z) = \begin{bmatrix} \tilde{h}_e(z) & \tilde{g}_e(z) \\ \tilde{h}_o(z) & \tilde{g}_o(z) \end{bmatrix}$$

Definition 2.1 If the determinant of the corresponding polyphase matrix $P(z)$ of filter pair (h, g) is 1, then we say filter pair (h, g) are complementary.

Theorem 2.2 (Lifting) Suppose filter pair (h, g) are complementary, any of the following form of limited filter g^{new} and h are complementary:

$$g^{new}(z) = g(z) + h(z)s(z^2)\ ,$$

where $s(z)$ is a polynomial of Laurent.

Theorem 2.3 (Dual lifting) Suppose filter pair (h, g) are complementary, any of the following form of limited filter h^{new} and g are complementary:

$$h^{new}(z) = h(z) + g(z)t(z^2)\ ,$$

where $t(z)$ is a polynomial of Laurent.

For all the polyphase matrices of filter bank $h(z)$, $g(z)$, $\tilde{h}(z)$, $\tilde{g}(z)$, there are:

$$P^{new}(z) = P(z)\begin{bmatrix} 1 & s(z) \\ 0 & 1 \end{bmatrix} \quad (3)$$

$$\tilde{P}^{new}(z) = \tilde{P}(z)\begin{bmatrix} 1 & 0 \\ -s(z^{-1}) & 1 \end{bmatrix} \quad (4)$$

where P^{new} and $\tilde{P}^{new}$ are the polyphase matrix and the dual polyphase matrix after lifting, respectively.

III 9/7 WAVELET FILTER DESIGN BASED ON THE LIFTING SCHEME

A. Wavelet Lifting from 5/3 to 7/5 filter

If the filters of a 5/3 wavelet are given by:

$$h(z) = h_2 z^{-2} + h_1 z^{-1} + h_0 + h_1 z + h_2 z^2,$$
$$g(z) = g_1 z^{-1} + g_0 + g_1 z,$$

their polyphase representations are, as follows:

$$h_e(z) = h_2 z^{-1} + h_0 + h_2 z\ ,$$

$$h_o(z) = h_1 + h_1 z\ ,$$

$$g_e(z) = g_0\ ,$$

$$g_o(z) = g_1 + g_1 z\ .$$

Applying the Euclidean algorithm to $\begin{cases} a_0(z) = h_e(z) \\ b_0(z) = h_o(z) \end{cases}$ may give in two steps the following quotients q_i and remainders $r_i (i = 1, 2)$:

$$\begin{cases} q_1(z) = \frac{h_2}{h_1}(1+z^{-1}) \\ q_2(z) = \frac{h_1}{h_0 - 2h_2}(1+z) \\ r_1(z) = h_0 - 2h_2 \\ r_2(z) = 0 \end{cases} \quad (5)$$

Given these quotients the polyphase matrix $P(z)$ can be factorized:

$$P(z) = \begin{bmatrix} h_e & g_e \\ h_o & g_o \end{bmatrix} = \prod_{i=1}^{2} \begin{bmatrix} q_i(z) & 1 \\ 1 & 0 \end{bmatrix} \begin{bmatrix} K & 0 \\ 0 & 1/K \end{bmatrix}, \quad (6)$$

where K is a constant scale factor.

For $\alpha = \frac{h_2}{h_1}$, $\beta = \frac{h_1}{h_0 - 2h_2}$, equation (6) gives the following polyphase matrix:

$$P(z) = \begin{bmatrix} h_e(z) & g_e(z) \\ h_o(z) & g_o(z) \end{bmatrix} = \begin{bmatrix} K(\alpha\beta z + 2\alpha\beta + 1 + \alpha\beta z^{-1}) & \alpha(1+z^{-1})/K \\ K\beta(1+z) & 1/K \end{bmatrix} \quad (7)$$

Let lifting operator $s(z)$ be:

$$s(z) = K^{-2}\gamma(1+z^{-1}), \quad (8)$$

where γ is a free parameter. The polyphose matrix $P^{new}(z)$ for the 7/5 filter can now be given by:

$$P^{new}(z) = P(z)\begin{bmatrix} 1 & s(z) \\ 0 & 1 \end{bmatrix} = \begin{bmatrix} h_e(z) & h_e(z)s(z) + g_e(z) \\ h_o(z) & h_o(z)s(z) + g_o(z) \end{bmatrix} \quad (9)$$

After lifting we obtain the new 7/5 filter coefficients:

$$\begin{cases} h_0 = (1+2\beta\gamma)/K \\ h_1 = (3\alpha\beta\gamma + \gamma + \alpha)/K \\ h_2 = \beta\gamma/K \\ h_3 = \alpha\beta\gamma/K \\ g_0 = (2\alpha\beta+1)K \\ g_1 = \beta K \\ g_2 = \alpha\beta K \end{cases} \quad (10)$$

Wavelet Lifting from 7/5 to 9/7 filter

If the filter of the 7/5 wavelet filter is

$$h(z) = h_3 z^{-3} + h_2 z^{-2} + h_1 z^{-1} + h_0 + h_1 z + h_2 z^2 + h_3 z^3,$$

$$g(z) = g_2 z^{-2} + g_1 z^{-1} + g_0 + g_1 z + g_2 z^2,$$

their polyphase representations are given by:

$$h_e = h_0 + h_2(z + z^{-1}),$$

$$h_o = h_1(z+1) + h_3(z^2 + z^{-1}),$$

$$g_e(z) = g_0 + g_2(z + z^{-1}),$$

$$g_o(z) = g_1 + g_1 z.$$

Again applying the Euclidean algorithm to $\begin{cases} a_0(z) = h_e(z) \\ b_0(z) = h_o(z) \end{cases}$ may give in four steps the following quotients q_i and remainders $r_i (i = 1,2,3,4)$:

$$\begin{cases} q_1(z) = 0 \quad , \quad r_1(z) = h_0 + h_2(z + z^{-1}) \\ q_2(z) = \frac{h_3}{h_2}(1+z) \quad , \quad r_2(z) = (h_1 - h_3 - \frac{h_0 h_3}{h_2})(1+z) \\ q_3(z) = \frac{h_2}{h_1 - h_3 - \frac{h_0 h_3}{h_2}}(1+z^{-1}) \quad , \quad r_3(z) = h_0 - 2h_2 \\ q_4(z) = \frac{h_1 - h_3 - \frac{h_0 h_3}{h_2}}{h_0 - 2h_2}(1+z) \quad , \quad r_4(z) = 0 \end{cases}$$

The corresponding polyphase matrix factorization is:

$$P(z) = \begin{bmatrix} h_e(z) & g_e(z) \\ h_o(z) & g_o(z) \end{bmatrix} = \prod_{i=1}^{4} \begin{bmatrix} q_i(z) & 1 \\ 1 & 0 \end{bmatrix} \begin{bmatrix} K & 0 \\ 0 & 1/K \end{bmatrix} \quad (11)$$

For $\alpha = \frac{h_3}{h_2}$, $\beta = \frac{h_2}{h_1 - h_3 - \frac{h_0 h_3}{h_2}}$, $\gamma = \frac{h_1 - h_3 - \frac{h_0 h_3}{h_2}}{h_0 - 2h_2}$, according to (10) we get the following matrix for $P(z)$:

$$P(z) = \begin{bmatrix} K(\beta\gamma z^{-1} + 2\beta\gamma + 1 + \beta\gamma z) & \beta(1+z^{-1})/K \\ K(\alpha\beta\gamma z^{-1} + 3\alpha\beta\gamma + \gamma + \alpha \\ +(3\alpha\beta\gamma + \gamma + \alpha)z + \alpha\beta\gamma z^2) & (\alpha\beta z^{-1} + 2\alpha\beta + 1 + \alpha\beta z)/K \end{bmatrix}$$

The filters $h(z)$ and $g(z)$ now follow from the polyphase form:

$$
\begin{aligned}
h(z) &= h_e(z^2) + z^{-1}h_o(z^2) \\
&= K(\beta\gamma z^{-2} + 2\beta\gamma + 1 + \beta\gamma z^2) \\
&\quad + z^{-1}K(\alpha\beta\gamma z^{-2} + 3\alpha\beta\gamma + \gamma + \alpha \\
&\quad + (3\alpha\beta\gamma + \gamma + \alpha)z^2 + \alpha\beta\gamma z^4) \\
&= K(\alpha\beta\gamma z^{-3} + \beta\gamma z^{-2} + (3\alpha\beta\gamma + \gamma + \alpha)z^{-1} \\
&\quad + 2\beta\gamma + 1 + (3\alpha\beta\gamma + \gamma + \alpha)z + \beta\gamma z^2 + \alpha\beta\gamma z^3)
\end{aligned}
$$

$$
\begin{aligned}
g(z) &= g_e(z^2) + z^{-1}g_o(z^2) \\
&= \beta(1 + z^{-2})/K \\
&\quad + z^{-1}(\alpha\beta z^{-2} + 2\alpha\beta + 1 + \alpha\beta z^2)/K \\
&= (\alpha\beta z^{-3} + \beta z^{-2} + (2\alpha\beta + 1)z^{-1} + \beta + \alpha\beta z)/K
\end{aligned}
$$

With the lifting operator with free parameter η given by the following equation

$$s(z) = K^{-2}\eta(1 + z^{-1}), \quad (12)$$

the new polyphase matrix is obtained as follows:

$$
\begin{aligned}
P^{new}(z) &= P(z)\begin{bmatrix} 1 & s(z) \\ 0 & 1 \end{bmatrix} \\
&= \begin{bmatrix} h_e(z) & h_e(z)s(z) + g_e(z) \\ h_o(z) & h_o(z)s(z) + g_o(z) \end{bmatrix}
\end{aligned}
$$

So, the resulting 9/7 coefficients after lifting are:

$$
\begin{cases}
h_0 = (6\alpha\beta\gamma\eta + 2\eta\gamma + 2\eta\alpha + 2\alpha\beta + 1)/K \\
h_1 = (3\beta\gamma\eta + \eta + \beta)/K \\
h_2 = (4\alpha\beta\gamma\eta + \gamma\eta + \alpha\eta + \alpha\beta)/K \\
h_3 = \beta\gamma\eta/K \\
h_4 = \alpha\beta\gamma\eta/K \\
g_0 = (1 + 2\beta\gamma)K \\
g_1 = (3\alpha\beta\gamma + \gamma + \alpha)K \\
g_2 = \beta\gamma K \\
g_3 = \alpha\beta\gamma K
\end{cases} \quad (13)
$$

According to the perfect reconstruction condition of 9/7 wavelet transform, wavelet properties, and normalizing condition, the above coefficients can be expressed in the form of a one-dimensional function:

$$
\begin{cases}
h_0 = -(8t^3 - 18t^2 + 7t - 20)/16t \\
h_1 = (4t^3 - 11t^2 + 15t - 4)/8t \\
h_2 = (t - 2)/4t \\
h_3 = (4t^2 - 7t + 4)(t - 1)/8t \\
h_4 = (4t^2 - 7t + 4)(2t - 1)/32t \\
g_0 = (t + 1)/4 \\
g_1 = (2t + 7)/32 \\
g_2 = -(t - 1)/8 \\
g_3 = -(2t - 1)/32
\end{cases} \quad (14)
$$

Based on equation (14), the range of t can be determined as $t \in [0.78, 1.85]$. If t is a known number, the filter coefficients can be easily be determined using equation (14), resulting in a newly designed 9/7 wavelet filter bank.

IV THE REGULARITY OF 9/7 WAVELET

The biorthogonal wavelet filter bank $\{h(z), g(z), \tilde{h}(z), \tilde{g}(z)\}$ must satisfy the regularity condition for image coding. Suppose L_1 and L_2 are the vanishing moments of lowpass filter on analysis and synthesis sides respectively, the dynamic range of the control variable t in equation (14) is determined by adopting Daubechies' theorem. We have the following equations:

$$
\begin{cases}
h(z) = \left[\dfrac{(1 + e^{-i\xi})}{2}\right]^{L_1} F(\xi) \\
g(z) = \left[\dfrac{(1 + e^{-i\xi})}{2}\right]^{L_2} Q(\xi)
\end{cases} \quad (15)
$$

where $z = e^{i\xi}$, $F(\xi)$ and $Q(\xi)$ are both trigonometric polynomial related with control variable. Concurrently, we get the following equations:

$$
\begin{cases}
B_k^1 = \max\limits_{\xi} |F(\xi)F(2\xi)\cdots F(2^{k_1 - 1}\xi)|^{1/k_1} < 2^{L_1 - 1/2} \\
B_k^2 = \max\limits_{\xi} |Q(\xi)Q(2\xi)\cdots Q(2^{k_2 - 1}\xi)|^{1/k_2} < 2^{L_2 - 1/2}
\end{cases}, \quad (16)
$$

where k_1 and k_2 are both Integer. The equation (16) gives a limiting condition of biorthogonal wavelet filter bank for image coding application, which leads to the determination of the dynamic range of the control variable t of the new 9/7 wavelet filter family designed in this paper, thus being capable of designing an optimal new 9/7 wavelet filter for image coding.

As to the new 9/7 wavelet filter designed in this paper, the values of its vanishing moments L_1 and L_2 are 2 and 4. If $k_1 = k_2 = 40$, according to the equation (16), the range of t can be determined as $t \in [0.78, 1.85]$. If t is determined, the filter coefficients can be obtained according to equation (14), thus the new 9/7 wavelet filter can also be determined.

V EXPERIMENT AND ANALYSIS

Taking the above one-dimensional parameterized 9/7 wavelet filter family as the coding kernel, adopting EBCOT (Embedded Block Coding with Optimized Truncation) coding [15], and applying this system to the image coding of Brodatz standard texture image database, it is found, by analysis of the experiment statistics in Fig. 1 and Fig. 2, that the control variable at the optimal PSNR is $t = 1.2050$. Therefore, our new 9/7 wavelet filter banks for texture image coding applications is known as given in Table1.

The 111 images in Brodatz standard texture image database are all tested based on the above image coding system. The results show that comparing the coding system of JPEG2000 with the coding system proposed in this paper, when compression rate is 4:1, the average PSNR value of the 111 texture image in Brodatz is only 0.0077dB lower than that of JPEG2000, with the PSNR of 49 images higher than that of JPEG200 at the average height of 0.0373dB, while the PSNR of 62 images are lower than that of JPEG2000 at the average amount of 0.0433dB.

When the compression rate are 8:1, 16:1, 32:1, 64:1, and 128:1, respectively, the results show in Table 2.

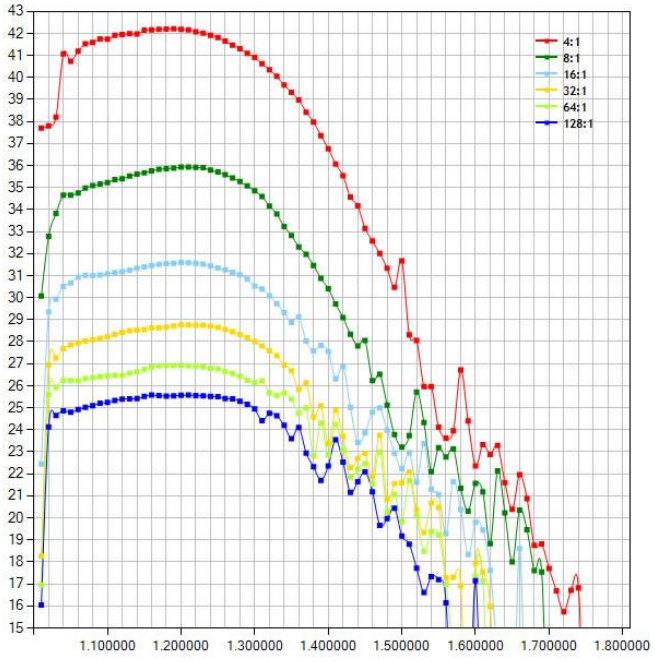

Figure 1. The PSNR value of test image D29 at the control variable's varying range of 1.000000-1.800000 under each compression ratio in the Brodatz standard texture image database

TABLE I. THE COEFFICIENTS OF NEW 9/7 WAVELET FILTER BANK ($t = 1.2050$)

k	Analysis filter coefficients		Synthesis filter coefficients	
	Low pass h_k	***High pass*** $\tilde{h}_k$	***Low pass*** g_k	***Hign pass*** $\tilde{g}_k$
0	0.5513	1.2295	1.2295	0.5513
± 1	0.2941	-0.5292	0.5292	-0.2941
± 2	-0.0256	-0.1649	-0.1649	-0.0256
± 3	-0.0441	-0.0292	0.0292	0.0441
± 4		0.0502	0.0502	

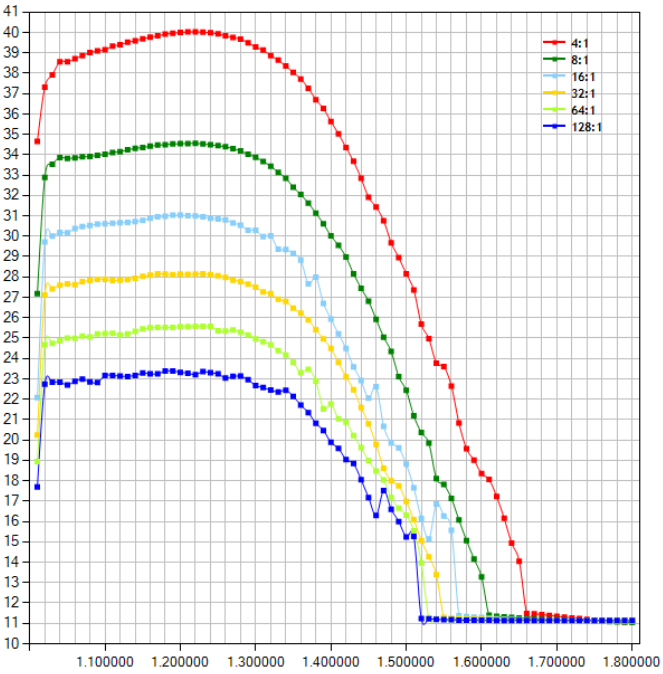

Figure 2. The PSNR value of image D110 at the control variable's varying range of 1.000000-1.800000 under each compression ratio in the Brodatz standard texture image database

The objective comparison of experimental statistic of maximum PSNR under different compression ratio for test images in the Brodatz standard texture image database are shown in Table 3.

The subjective comparison of compression performances between our new 9/7 filter and CDF 9/7 for test images D29, D43, D84 and D103 in the Brodatz standard texture image database under compression ratio 32:1 are shown in Figure 3, Figure 4 and Figure 5.

The images in Fig.4 are the reconstructed images of the above four images through the compression experiments by JPEG2000 standard CDF 9/7 filter at the compression ratio of 32:1.

The images in Fig.5 are the reconstructed images of same four images from the Brodatz standard texture image database, but through the compression experiments by the new 9/7 filter designed in this paper at the compression ratio of 32:1.

From comparison of Fig.4 and Fig.5, the resulting subjective visual quality of reconstructed images using the new 9/7 filter is concluded to be as good as the quality resulting from using the CDF 9/7 filter.

TABLE II. COMPARISON OF THE COMPRESSION PERFORMANCES BETWEEN NEW 9/7 AND CDF 9/7 FILTER (PSNR/DB)

Image Database	Compression Ratio	Total amount of images	Mean differences	Image number	Mean differences	Image number	Mean differences
Brodatz	4:1	111	-0.0077	49	+0.0373	62	-0.0433
Brodatz	8:1	111	+0.0014	52	+0.0262	59	-0.0205
Brodatz	16:1	111	+0.0028	64	+0.0231	47	-0.0248
Brodatz	32:1	111	+0.0207	75	+0.0483	36	-0.0369
Brodatz	64:1	111	+0.0330	82	+0.0593	29	-0.0415
Brodatz	128:1	111	+0.0482	70	+0.1072	41	-0.0525

TABLE III. EXPERIMENT STATISTICS OF MAXIMUM PSNR FOR DIFFERENT COMPRESSION RATIOS

Compression Ratio	Image	CDF9/7 wavelet	New 9/7 wavelet	Difference
4:1	D110	27.595602	27.670151	+0.074549
	D71	32.500939	32.574722	+0.073783
	D91	44.501023	44.570713	+0.069690
	D52	34.765339	34.833791	+0.068452
8:1	D103	22.897491	22.982836	+0.085345
	D5	28.339782	28.408767	+0.068985
	D47	35.412800	35.480066	+0.067266
	D2	26.703806	26.761880	+0.058074
16:1	D47	30.651179	30.727201	+0.076022
	D62	31.821213	31.886339	+0.065126
	D98	30.184702	30.247055	+0.062353
	D38	26.300726	26.354982	+0.054256
32:1	D103	15.796872	15.982187	+0.185315
	D84	18.952107	19.079902	+0.127795
	D29	21.238714	21.347855	+0.109141
	D43	28.080872	28.189965	+0.109093
64:1	D87	15.424513	15.692062	+0.267549
	D30	28.624222	28.829037	+0.204815
	D102	17.269489	17.456338	+0.186849
	D18	21.291975	21.457116	+0.165141
128:1	D53	13.688657	14.018516	+0.329859
	D65	17.517933	17.817868	+0.299935
	D68	18.748988	19.044899	+0.295911
	D46	23.911123	24.167780	+0.256657

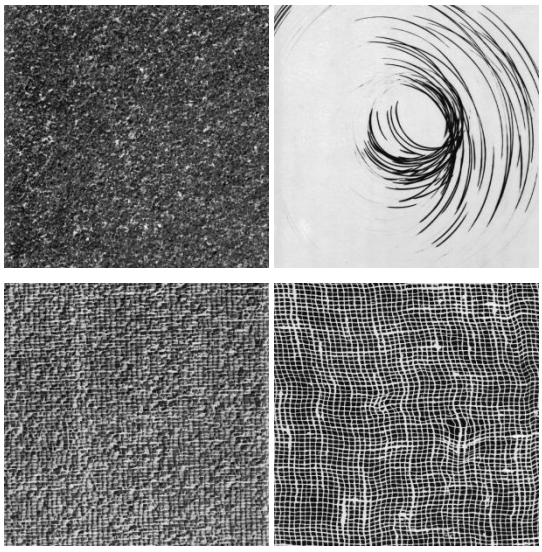

Figure 3. Original four images, Top: D29 and D43, Bottm: D84 and D103

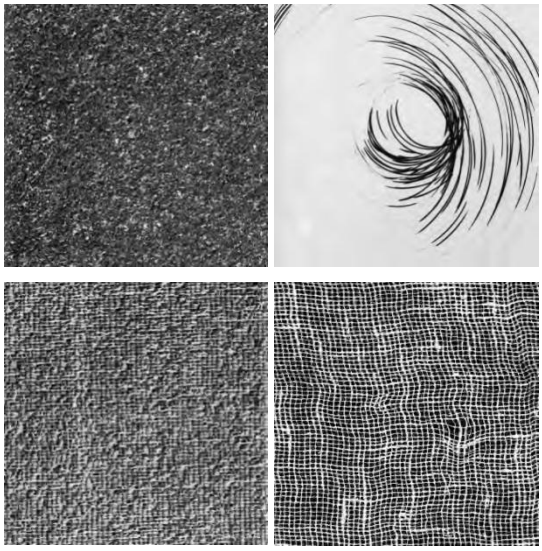

Figure 4. The reconstructed images, Top: D29 and D43, Bottm: D84 and D103, CDF9/7, CR=32:1

VI. CONCLUSION

Compared with CDF 9/7 wavelet filter, the new 9/7 wavelet filter designed in this paper is much easier to be constructed and more favorable in hardware implementation. The results show that under high compression ratio (low bit rate), the overall coding performance of the new 9/7 wavelet filter is better than that of the JPEG2000 CDF9/7 wavelet filter, therefore, the 9/7 wavelet filter designed in this paper is very effective in image coding for texture image.

ACKNOWLEDGMENT

This work was supported by the Chinese national natural science foundation under grant 51075317, and project 973 of national key basic research of China under grant 2007CB311005.

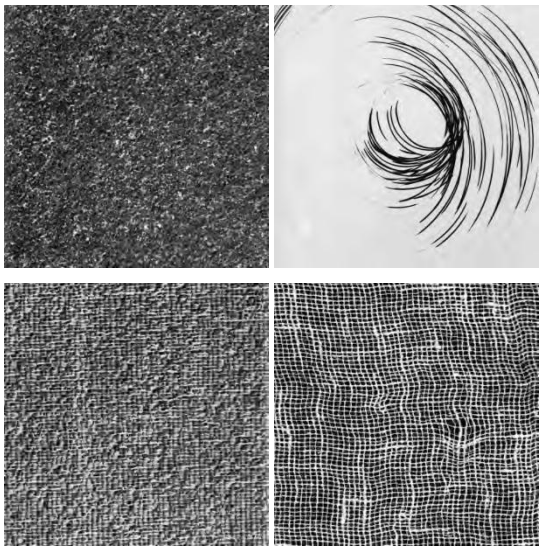

Figure 5. The reconstructed images, Top: D29 and D43, Bottm: D84 and D103, new 9/7, CR=32:1

REFERENCES

[1] M. Vertterli, and J. Kovacevic, Wavelet and subband coding. Prentice Hall, Englewood Cliffs, New Jersey, 1995.

[2] M. Vetterli, and C. Herley, "Wavelets and Filter Banks: Theory and Design," IEEE Transactions on Signal Processing, vol.40, 1992, pp.2207-2232.

[3] A. Cohen, I. Daubechies, and J. Feauveau, "Biorthogonal bases of compactly supported wavelets," Communications on Pure and Applied Mathematics, vol.45, 1992, pp.485-560.

[4] W. Sweldens, "The lifting scheme: a construction of second generation wavelets," SIAM Journal on Mathematical Analysis, vol.29, 1997, pp.511-546.

[5] W. Sweldens, "The lifting scheme: a custom-design construction of biorthogonal wavelets," Applied and Computational Harmonic Analysis, vol.3, 1996, pp.186-200.

[6] I. Daubechies, and W. Sweldens, "Factoring Wavelet Transforms into Lifting Steps," The Journal of Fourier Analysis and Applications, vol.4, 1998, pp.247-269.

[7] L. Cheng, D.L. Liang, and Z.H. Zhang, "Popular biorthogonal wavelet filters via a lifting scheme and its application in image compression," IEE Proceedings Vision, Image and Signal Processing, vol.150, 2003, pp.227-232.

[8] Guoan Yang, and Nanning Zheng, "An Optimization Algorithm for Biorthogonal Wavelet Filter Banks Design," International Journal of Wavelets, Multiresolution and Information Processing, vol.6, 2008, pp.51-63.

[9] Guoan Yang, Nanning Zheng, and Shugang Guo, "Optimal Wavelet Filter Design for Remote Sensing Image Compression," Journal of Electronics (China), vol.24, 2007, pp.276-284.

[10] See-May Phoong, C.W. Kim, P.P. Vaidyanathan, and R. Ansari, "A new class of two-channel biorthogonal filter banks and wavelet bases," IEEE Transactions on Signal Processing, vol.43, 1995, pp.649-665.

[11] M. Antonini, M. Barlaud, P. Mathieu, and I. Daubechies, "Image coding using wavelet transform," IEEE Transactions on Image processing, vol.1, 1992, pp.205-220.

[12] Dong Wei, Jun Tian, R.O. Wells, and C.S. Burrus, "A new class of biorthognal wavelet systems for image transform coding," IEEE Transactions on Image processing, vol.7, 1998, pp.1000-1013.

[13] Zaide Liu, Nanning Zheng, Yuehu Liu, and Huub van de Wetering, "Optimization Design of Biorthogonal Wavelets for Embedded Image Coding," IEICE Transactions on Information and Systems, vol.E90-D, 2007, pp.569-578.

[14] Do Quan, and Yo-Sung Ho, "Efficient Wavelet Lifting Scheme Based on Filter Optimization and Median Operator," IEEE-RIVF International Conference on Computing and Communication Technologies, Da Nang Univ Technol, Da Nang, Vietnam, 2009, pp.284-289.

[15] D. Taubman, "High performance scalable image compression with EBCOT," IEEE Transactions on Image processing, vol.9, 2000, pp.1158-1170.

[16] A. Said, and W.A. Pearlman, "A new fast and efficient image codes based set partitioning in hierarchical trees," IEEE Transactions on Circuits and Systems for Video Technology, vol.6, 1996, pp.243-250.

[17] L. F. Villemoes, "Energy Moments in Time and Frequency for Two-Scale Difference Equation Solutions and Wavelets," SIAM Journal on Mathematical Analysis, vol.23, 1992, pp.1519-1543.

[18] A. Cohen, and I. Daubechies, "A Stability Criterion For Biorthoronal Wavelet Bases And Their Related Subband Coding Scheme," DUKE Mathematical Journal, vol.68, 1992, pp.313-335.

[19] M. Unser, and T. Blu, "Mathematical properties of the JPEG2000 wavelet filters. IEEE Transactions on Image processing, 2003, 12(9): 1080-1090.

[20] J. D. Villasenor, B. Belzer, and J. Liao, "Wavelet filter evaluation for image compression," IEEE Transactions on Image Processing, vol.4, 1995, pp.1053-1060.

[21] Yi Shang, Longzhuang Li, and Benjamin Wah, "Optimization design of biorthogonal filter banks for image compression," Elsevier Information Sciences, vol.132, 2001, pp.23-51.

Mesopic Visual Performance of Cockpit's Interior based on Artificial Neural Network

Dongdong WEI
Fudan University
Dept of Mechanics & Science Engineering
Shanghai, China

Gang SUN
Fudan University
Dept of Mechanics & Science Engineering
Shanghai, China

***Abstract*— The ambient light of cockpit is usually under mesopic vision, and it's mainly related to the cockpit's interior. In this paper, a SB model is come up to simplify the relationship between the mesopic luminous efficiency and the different photometric and colorimetric variables in the cockpit. Self-Organizing Map (SOM) network is demonstrated classifying and selecting samples. A Back-Propagation (BP) network can automatically learn the relationship between material characteristics and mesopic luminous efficiency. Comparing with the MOVE model, SB model can quickly calculate the mesopic luminous efficiency with certain accuracy.**

Keywords- component; Mesopic Vision; Cockpit; Artificial Neural Network; BP; SOM.

I. INTRODUCTION

A. Cockpit's Interior Ergonomics

Visual comfort occupies an increasing important place in our everyday life, but also in the field of aeronautics which is the subject of this paper. Modern science and technology is people-oriented. More and more human factors were taken into consideration on the development of modern civil airplane.

A subject of applying ergonomics into man-machine relationship develops gradually, which has brought about more and more attention. The ambient light of cockpit consists of natural sunlight, instruments panels, inside lighting systems and interior's reflecting light. The quality of ambient light in the man-machine system should meet the requirements, as well as providing people visual information about activity both in quality and quantity. It should meet ergonomics requirements of perceptive information, aiming at making people comfortable and pleasant.

The cockpit's comfort plays an important role in pilot's job, especially the visual performance. About 80% outside information is received though vision, which makes vision the most important channel to communicate with external world [1]. Visual comfort is the psychological feeling about comfort level in ambient light. So, visual comfort is a quantity of psychological feeling.

Uncomfortable vision will cause a series of symptoms, usually appears as redness and swelling, pain, itching, tears, dizziness or even intestines and stomach problems. Comfortable environment of cockpit would guarantee the pilot keep a normal state in the process of work, to avoid flight accidents caused by visual factors.

In the man-machine ergonomics study, establish the inner relationship between different materials properties and light source, and the received luminance, light intensity, contrast and color in the specific conditions. Simulate different characteristics of efficiency of different light source and different materials. The influences of these multidisciplinary factors are not independent. They're of complicated nonlinear relation. Past studies domestic and oversea are mostly aimed at single factor of variables, without considering the nonlinear relationship between multiple factors and the coupling mechanism.

The established design standards and norms cannot completely meet the pilot's ergonomics requirements in the real flight environment, thus increasing the design difficulty of a cockpit ergonomics system. There's a long history according to the visual ergonomics research in cockpit. Britain and America have already done a lot of experimental and theoretical research, and established design standards of illumination and colorimetry. However, there's only a little study for the interior system of ergonomics problem. The domestic related research is scattered, mainly paused in the qualitative subjective evaluation level, which cannot form a systematic theory. Through the research of aircraft cockpit's coupling mechanism, characteristics of the pilot's visual perception and comprehensive effect with multivariable factors, we can build the civil aircraft cockpit's interior ergonomics theory model and application mechanism.

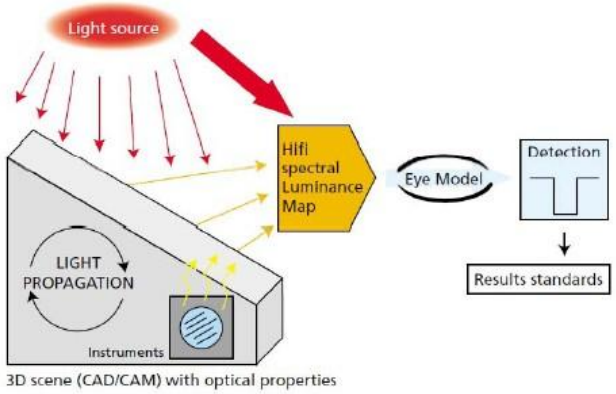

Figure 1. Cockpit's visual system model

OPTIS established a cockpit's visual system model [2] by CATIA based on ergonomic design criteria and a certain type of aircraft cockpit, which is shown in Figure.1. Then various optical properties could be set, including the characteristics of

light source spectral and optical materials which participating in the process of light transmission. After that, they can be applied to the optical tracking system to simulate the light process.

For safety reasons, visual information must be seen as comfortable as possible by the aircraft pilot in any light conditions. In this paper, we focus on the cockpit's mesopic visual performance based on the ANN method.

B. Mesopic Vision

Mesopic light levels are those between the photopic (daytime) and scotopic (extremely low) light levels. The mesopic luminance range covers brightness between about 0.001 and 3 cd/㎡. Most night-time outdoor and traffic lighting environments and some indoor lighting are in the mesopic range [3].

As human eyes have different perceptions on light fusions from different frequency, there comes to be different brightness, for observers, between lights of different wavelength even with the same power. Luminous efficiency function curves indicate such a human eye character.

Photopic luminous efficiency function $V(\lambda)$ (in Figure2) , which is fit for delineating the spectral response within a 2-degree range of human eyes in a higher brightness, is the most widely used function in this field and was brought forward on the 6th conference of CIE in 1924. CIE has successively brought forward the function with a wider range of 10 degree and also the luminous efficiency function $V'(\lambda)$ for environments of low brightness less than 0.001cd/㎡.

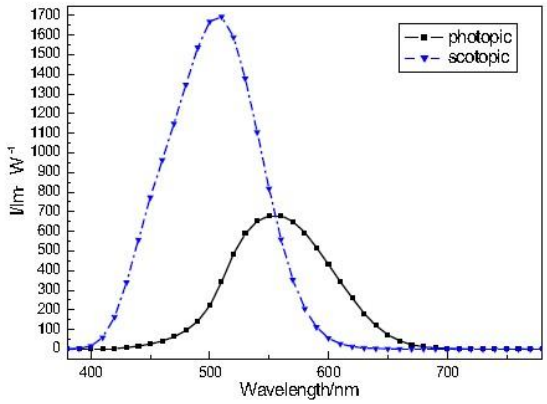

Figure 2. Photopic luminous efficiency function $V(\lambda)$ and scotopic luminous efficiency function $V'(\lambda)$.

Mesopic photometry has a long history. Most mesopic photometry models have concentrated on brightness evaluation. The early works began in the 1950s and then a special research put forward by the Committee of Mesopic Version Photometry in CIE started in 1983. A number of studies of visual performance at mesopic light levels have been conducted, which underscore the importance of recognizing the distinction between photometry and a complete characterization of visual responses at mesopic levels [4]. The EC project MOVE [5] (Mesopic Optimisation of Visual Efficiency) was carried out during 2002-2004 in the EC Fifth Framework programme (G6RD-CT-2001-00598). The objective of the project was to define relevant spectral sensitivity functions for the luminance range of 0.01 – 10 cd/㎡, where standardisation is most urgently needed. The TC1-58 Technology Committee found in 2000 also by CIE came up with a better model using the method of visual performance and such a function below was brought forward [6]:

$$M_m V_m(\lambda) = xV(\lambda) + (1-x)V'(\lambda) \quad (1)$$

Where $V_m(\lambda)$ represents the mesopic luminous efficiency function under the environment of a certain backdrop brightness, M_m is the normalization factor of $V_m(\lambda)$, x is a parameter which is located between 0 and 1 based on backdrop brightness and spectral power. x=1 is in photopic conditions while x=0 in scotopic conditions.

Illumination is defined as the transparent flux on unit area, and flux is available from function below:

$$\phi_x = M_x \int_{380}^{780} P(\lambda) \cdot V_x(\lambda) d\lambda \quad (2)$$

Where ϕ_x stands for the total flux, $P(\lambda)$ is the spectral arrangement function of light source, $V_x(\lambda)$ is the luminous efficiency function on certain brightness, M_x is the normalization factor. $s/p = \phi_s / \phi_p$.

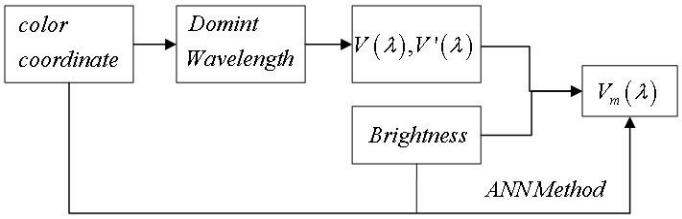

Figure 3. The process of calculating

In this paper, a new method has been used into human vision model to simplify the nonlinear relationship between light characteristics and mesopic vision. In real time scenario, there are many factors taken into consideration. However, we focus on some dominant variable in this paper.

II. ARTIFICIAL NEURAL NETWORK

An artificial neural network (ANN), usually called neural network (NN), is a mathematical model or computational model that is inspired by the structure and/or functional aspects of biological neural networks. A neural network consists of an interconnected group of artificial neurons, and it processes information using a connectionist approach to computation.

From 1940s, with human being's fully understanding of the brain structure, composition and the most basic unit, Artificial Neural Network was arose [7]. Simplified model

(ANN) was established after combining mathematics, physics and information processing method, and making neural network abstracted.

As an active marginal subject, the research and application of neural network is becoming a hot pot of artificial intelligence, cognitive science, neurophysiology, nonlinear dynamics, and other related subjects. In last ten years, academic research according to neural network is very active, and puts forward almost a hundred of neural network model. Neural network is also widely used in analysis of input and output with multiple variables. In the process of aircraft design, using the neural network to optimize pneumatic parameters has obtained some progress.

In this paper, SOM network is used to compress a set of high-dimensional input parameters that contain material characteristics onto a two-dimensional SOM grid. SOM network is different from other artificial neural networks in the sense that it uses a neighborhood function to preserve the topological properties of the input space. The neurons will classify the space, each neuron representing a partition of that space.

SOM network employs an Winner-Takes-All (WTA) operation, which only the winner is allowed to adjust the weight connecting to the input. The training process includes sequential steps[8].

a) Initialization: Randomly specify the weight value $W_j, j=1,2,\cdots,m$ (m stands for the number of neurons on competitive layer) and give the initial value of Learning Rate $\eta(0)$ and Radius of Neighbor $N_{j^*}(0)$.

b) Competition: Select a certain sample:

$$X^p=\left(X_1^p, X_2^p,\cdots, X_n^p\right) \tag{3}$$

Then calculate the responses by (4) to all the neurons on competitive layer. Find the winning neuron j^* with the largest response.

$$Y_j=W_j^T X^p,\ j=1,2,\cdots,m \tag{4}$$

c) Adaption: Calculate the radius of neighbor neurons $N_{j^*}(t)$, and all neuron weights in the radius will be adjusted by (2).

$$\begin{aligned} &w_{ij}(t+1)=w_{ij}(t)+\eta(t,N)\left[x_i^p-w_{ij}(t)\right] \\ &i=1,2,\cdots,n;\ j\in N_{j^*}(t) \end{aligned} \tag{5}$$

Where the Learning Rate η will be the function of training time t and the radius of neighbor N

$$\eta(t,N)=\eta(t)e^N$$

$$\eta(t)=\begin{cases}\eta_0, & t\le t_p\\ \eta_0\left(1-\dfrac{t-t_p}{t_m-t_p}\right), & t_p<t\le t_m\end{cases} \tag{6}$$

In which, t_m is the total cycles for training and t_p is the cycle time keeping the original learning rate. If $\eta(t)$ declines to a tolerance or the training time t is long enough, then the training is finished, or else go to step b) continuing another sample.

After the whole training, the network will be sensitive differently to the samples in database. The samples with close characteristics will generate similar response on the output map, which proves to classify different types of samples successfully.

BP network model is the most typical artificial neutral network (ANN) model, widely used as a multi-layer feed-forward network, which includes input layer, hidden layer and output layer. In this paper, we give color coordinate and brightness as input and mesopic luminous efficiency function as teacher signal, so that the network will be capable of estimating any mesopic luminous efficiency by giving a single light characteristics. The training process follows 7 steps:

a) Initial all network weights to small random values.

b) Input a certain sample $X^p=\left(X_1^p, X_2^p,\cdots, X_n^p\right)$ to the network, and calculate the output of all the neurons.

c) For each neuron k on output layer ($l=L$), calculate the error term $\delta_k^{(L)}$.

$$\delta_k^{(L)}=(t_k-o_k)o_k(1-o_k) \tag{7}$$

d) Where, t_k is the teacher signal and o_k is the output of neuron k.

e) For each neuron on hidden layer ($2\le l\le L-1$), calculate the error terms $\delta_j^{(L)}$.

$$\delta_j^{(l)}=o_j(1-o_j)\sum_k \delta_k^{(l+1)} w_{kj}^{(l+1)} \tag{8}$$

f) Update the network weights as follows:

$$w_{jk}^{(l)}(n+1)=w_{jk}^{(l)}(n)+\eta\delta_j^{(l)}(n)o_k^{(l-1)}(n) \tag{9}$$

g) Go to step b) for another input sample until the termination condition is met.

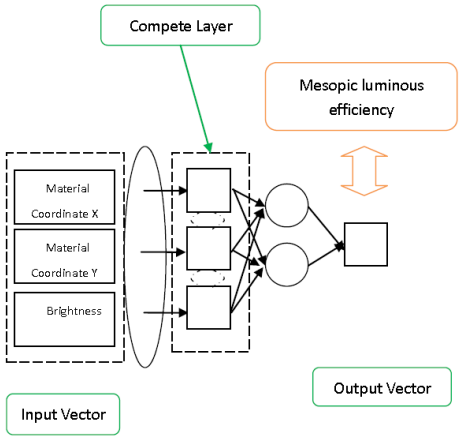

Figure 4. SB model

A new model combines SOM and BP network named SB model, shown as in Figure 4. It uses SOM to classify different samples while BP network to simulate nonlinear relationship between material characteristics and mesopic luminous efficiency.

III. EXPERIMENTAL RESULTS

To study the mesopic vision performance of pilot in cockpit, we gathered measurement variable into an initial database, shown as in Figure 5. In the condition of experiment, input variable including material reflectivity, material transmissivity, material absorptivity, luminous flux, color temperature, material coordinate x and material coordinate y, as well as output variable including brightness, light intensity, contrast, color x and color y.

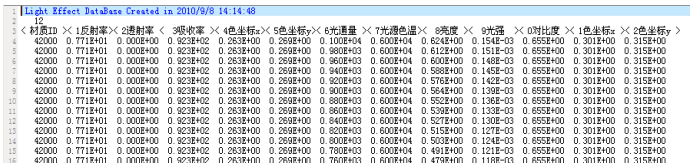

Figure 5. Initial database

After observing, material reflectivity, material transmissivity, and light intensity are invalid. In the condition of color temperature equals 5000K and luminous flux equals 1000lm. Initial database can be trimmed. The sample database shows as Figure 6.

Material Absorption	Material color X	Material color Y	Luminous Flux	Brightness	Luminous Intensity	Contrast	Color x	Color y
92.288	0.263	0.269	300	1.74E-01	4.29E-05	0.6207	0.307	0.321
73.521	0.287	0.307	280	7.55E-01	1.86E-04	0.3778	0.314	0.332
95.429	0.262	0.252	260	5.70E-02	1.40E-05	0.6731	0.306	0.316
86.685	0.253	0.267	240	2.66E-01	6.55E-05	0.4792	0.304	0.321
80.377	0.289	0.303	220	4.64E-01	1.14E-04	0.3524	0.315	0.331
72.87	0.291	0.292	200	5.01E-01	1.23E-04	0.3422	0.315	0.327
94.207	0.324	0.282	180	8.63E-02	2.13E-05	0.6162	0.329	0.323
75.061	0.264	0.265	160	3.59E-01	8.83E-05	0.4206	0.307	0.32
97.864	0.321	0.331	140	2.92E-02	7.19E-06	0.7294	0.325	0.338
85.827	0.304	0.312	120	1.64E-01	4.05E-05	0.473	0.32	0.333
94.768	0.316	0.329	100	5.39E-02	1.33E-05	0.6515	0.323	0.337
69.765	0.317	0.327	80	2.49E-01	6.14E-05	0.3416	0.324	0.337
96.286	0.317	0.325	60	1.18E-02	2.90E-06	0.6541	0.324	0.337
48.836	0.31	0.316	40	2.14E-01	5.28E-05	0.3056	0.322	0.334
59.569	0.338	0.356	20	8.70E-02	2.14E-05	0.3747	0.33	0.345

A. Dominant Wavelength

Calculate the dominant wavelength with x-y chromaticity coordinates in a Chromaticity Diagram [9], just illustrated in Figure 7.

Construct a line between the chromaticity coordinates of the reference white point on the diagram (for instance, CIE-E) and the chromaticity coordinates, and then extrapolates the line from the end that terminates at the filter point. The wavelength associated with the point on the horseshoe-shaped curve at which the extrapolated line intersects is the dominant wavelength. Table 1 gives some common illuminants used as a white reference.

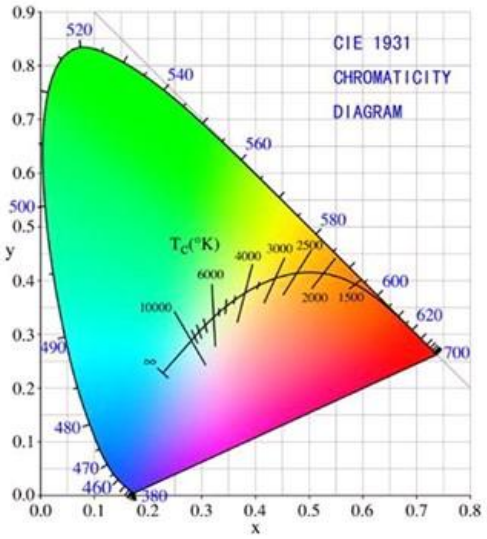

Figure 7. CIE 1931 Chromaticity Diagram

Chromaticity coordinates of some common illuminants used as a white reference.

TABLE I.

Reference White	x coordinate	y coordinate
CIE-E	0.3333	0.3333
CIE-A	0.4476	0.4075
CIE-C	0.3100	0.3162
CIE-D65	0.3127	0.3291

After calculation, the dominant wavelengths of color coordinates are shown in Table 2.

TABLE II. DOMINANT WAVELENGTH OF COLOR COORDINATES

color x	color y	wavelength
0.301	0.315	589
0.308	0.326	597
0.300	0.310	582
0.299	0.315	589
0.308	0.325	599
0.309	0.321	588
0.320	0.317	565
0.301	0.314	580
0.318	0.332	606
0.313	0.327	598
0.316	0.331	609
0.317	0.331	610
0.316	0.330	592
0.315	0.328	597
0.323	0.339	496

B. Mesopic Luminous Efficiency

Then the photopic luminous efficiency and the scotopic luminous efficiency could be obtained by dominant wavelength. The parameter x in formula (1) could be calculated according to Table 4 in reference [5].

According to the brightness and s/p ratios, x could be approximately calculated in certain conditions as shown in Table 2. The s/p ratio is chosen in the condition of typical overcast sky, which is 2.36 [10].

Linear fitting function's used to fulfill the x-value.

TABLE III. X-VALUE FOR MOVE MODEL

wavelength	brightness	x
589	0.6238	0.7721
597	2.8570	0.7977
582	0.2355	0.7660
589	1.1880	0.7799
599	2.2330	0.7917
588	2.6500	0.7958
565	0.5073	0.7703
580	2.3860	0.7933
606	0.2196	0.7657
598	1.4430	0.7830
609	0.5664	0.7712
610	3.2440	0.8012
592	0.2063	0.7655
597	5.5430	0.8229
496	4.4610	0.8120

$M(x)$ is a normalizing function such that $V_m(\lambda)$ attains a maximum value of 1, shown as in Figure 8.

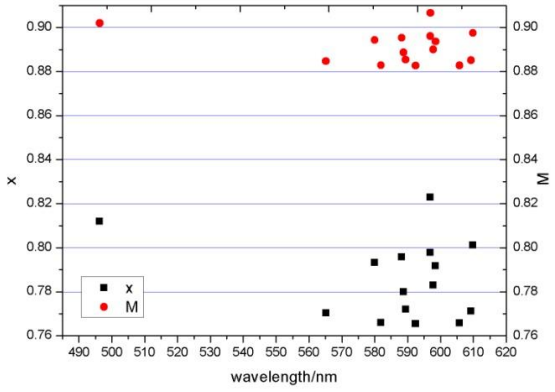

Figure 8. x-value and $M(x)$ distribution results

The MOVE model is applicable for other conditions such as typical sunlight sky and typical direct sunlight sky.

C. SOM Network Results

According to the design requirement, a total of 12 samples are selected, including brightness, color x and color y.

For initialization, we give the initial learning rate $\eta(0)_0 = 0.95$. And the radius of neighbor is defined as following expression:

$$N(t) = 0.9\exp(-10t / t_m = 2000) \quad (10)$$

According to the test result, total cycles of training t_m is defined as 20000.

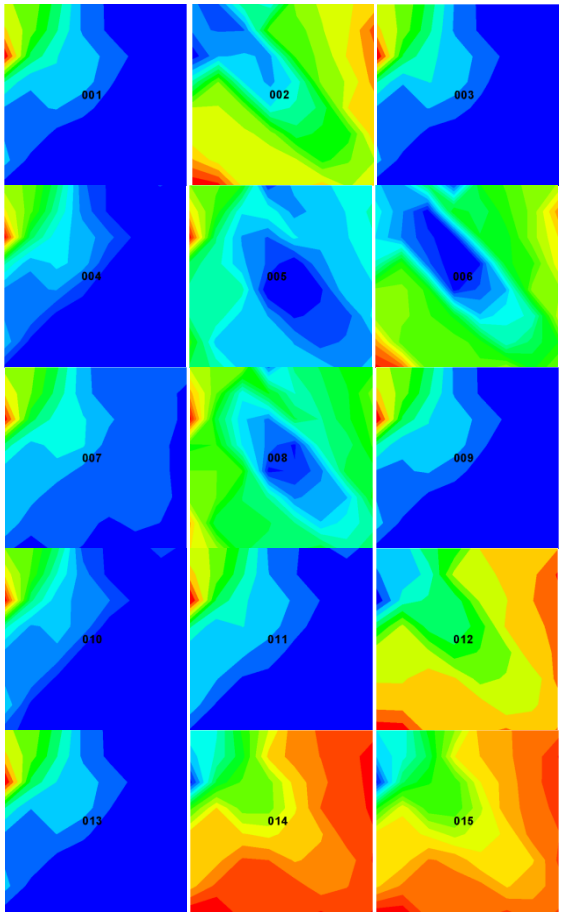

Figure 9. 2d-response by SOM

After the whole training, all 12 samples are classified into 4 groups on a 2×2 map. Table 4 shows the resulting SOM with cluster groups considering the all 3 characteristics. Figure 9 demonstrates the responses to different samples. The number is ranked from left to right and up to down, sign as 001 to 012. The more similar the characteristics of samples are, the closer the colored maps are.

From the colored result, we can easily get that most of the samples performed like the same in group 1. No.012, 014 and 015 are the most distinguishing ones.

TABLE IV.

Group 1	Group 2	Group 3	Group 4
001, 003,004 007,009,010 011,013	002	005, 006 008	012,014,015

D. BP Network Results

Construct a BP network, with color coordinate and brightness as input and mesopic luminous efficiency as teacher signal (target). The number of hidden nodes depends on the number, scale and complexity of samples. To confirm the number of hidden nodes, we take the formula as follow:

$$m = \sqrt{n + l} + \alpha \quad (5)$$

where m is the number of hidden nodes, n is the number of input nodes, l is the number of output nodes, and α is a constant between 1 and 10.

The main parameters of BP network are of $m = 3$ (hidden nodes), $lr = 0.15$ (learning ratio), $mingrad = 1e\text{-}10$ (minimum gradient), and $epochs = 100$.

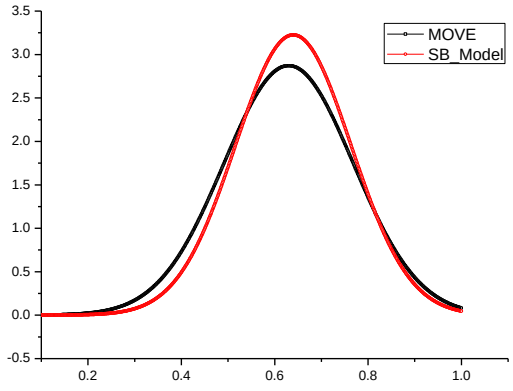

Figure 10. Error density distribution function

After the whole training, the result is shown in Figure 10. The black square line represents error density distribution function of MOVE model, as well as the red circle line represents error density distribution function of SB model. Observing the peak of these two models, mesopic luminous efficiency function of SB model is more concentrated than MOVE model.

CONCLUSIONS

This paper put forward a SB model, which uses SOM network to classified different samples into different groups. Chose a certain group, the training result is better than before. Use BP network to simplify the relationship between the mesopic luminous efficiency, and the different photometric and colorimetric variables in the cockpit. After comparing with the MOVE model, SB model takes advantage of ANN to simplify the relationship, and convenient to calculate mesopic luminous function, as well as has more concentrate error density distribution. To make research more accurate, we will take more research on simulating human's eye, and construct corresponding model. Photopic vision and scotopic vision are taken into consideration in the next as well.

ACKNOWLEDGMENT

The work is sponsored by National Basic Research Program ("973" Program) of China, Issue Number 2010CB734106.

REFERENCES

[1] Wei Liu, Xiugan Yuan, Haiyan Lin, Synthetical Evaluation of Ergonomics Study in Visual Information Flow System of Pilots, Journal of Beijing University of Aeronautics and Astronautics, 27(2), 2001.

[2] Jacques Delacour, Development of a new simulation software for visual ergonomy of a cockpit, Optis Corporation, 2002

[3] Yandan Lin, Dahua Chen, Wencheng Chen, The significance of mesopic visual performance and its use in developing a mesopic photometry system, Building and Environment, 41, 2006, 117-125.

[4] MS Rea, JD Bullough, JP Freyssinier-Nova, and A Bierman, A proposed unified system of photometry, Lighting Research and Technology, June 2004; vol. 36, 2: 85-109.

[5] Eloholma M, HMonen L, Performance based model for mesopic photometry, MOVE Project Report, 2005，Finland.

[6] Yong Yang, Zuojun Bao, Chuanzheng Zhu, Lei Wang, Study on the Mesopic Vision Theory Used in Road Tunnel Lighting Measurement, 2011 Third International Conference on Measuring Technology and Mechatronics Automation.

[7] Daqi Zhu, The Research Progress and Prospects of Artificial Neural Networks, Journal of Southern Yangtze University (Natural Science Edition), 3(1), 2004

[8] Jie Chen, Gang Sun, Xin Jin, Intelligent Aerodynamic Design for Airfoil Based on Artificial Neural NetworkMethod, Computer and Automation Engineering (ICCAE), 2010 The 2nd International Conference on, Feb. 2010, 289-293.

[9] Turan Erdogan, How to calculate luminosity, dominant wavelength, and excitation purity, Semrock White Paper Series

[10] S.M. Berman, Energy Efficiency Consequences of Scotopic Sensitivity, Journal of the Illuminating Engineering Society, 1992

Visual Working Efficiency Analysis Method of Cockpit Based On ANN

Yingchun CHEN
Commercial Aircraft Corporation of China,Ltd
Shanghai, China

Dongdong WEI
Fudan University
Dept. of Mechanics an Science Engineering
Shanghai, China

Gang SUN
Fudan University
Dept. of Mechanics and Science Engineering
Shanghai, China

***Abstract*— The Artificial Neural Networks method is applied on visual working efficiency of cockpit. A Self-Organizing Map (SOM) network is demonstrated selecting material with near properties. Then a Back-Propagation (BP) network automatically learns the relationship between input and output. After a set of training, the BP network is able to estimate material characteristics using knowledge and criteria learned before. Results indicate that trained network can give effective prediction for material.**

Keywords- component; Visual Working Efficiency; Artificial Neural Networks;Cockpit; BP; SOM.

I. INTRODUCTION

Modern science and technology are people-oriented. Taken more and more human factors into consideration on the development of modern civil airplane, a subject of applying ergonomics into man-machine relationship develops gradually, which has brought about more and more attention.

In the study of man-machine environment system, ergonomics experienced three phases, which were people-adapted-to-machine, machine-adapted-to-man and man-machine mutual adaptation [1]. Now it has already gone deep into a man-machine environment system of people, machine and environment coordinating with each other. In this system, purely studying on individual physiological and psychological characteristics has been developed into studying on how to improve a person's social factors. With market competition intensified and production level advanced, application of ergonomics in the design and manufacturing of mechanical products also is more wide and deep.

In the man-machine system, the size of each component of human body, the normal physiological values of man's vision and audition, the pose of man in work, human activities range, action rhythm and speed, fatigue degree caused by working conditions, and one's energy consumption and supplement; machine monitor, controller (handle, joysticks, steering wheel, button's structure and tonal, etc.), and various equipment (chair, table, etc.) associated with other people; environment temperature, humidity, noise, vibration, lighting, color, smell, etc will affect one person's working efficiency. Man-machine ergonomics is a subject studying the relationship of them.

Research direction of Man-machine ergonomics mainly displays in the following respects: visual factor (harmonious and pleased environment in both inside and outside cockpit), audition factor (quiet cockpit and cabin), tactile factor (comfortableness of seat and flight equipment), space factor (wild and uncrowded space of cockpit), and the relationship of safety, high efficiency and comfort.

The visual factor plays a very important role among them accounting for the fact that vision is the most important channel communicated with external world for people. About 80% information received from outside is obtained through the visual pathway. The main interface between man and machine in man-machine system is visual displayer [2]. Results have shown that, warm color causes eyes fatigue easier than cool color. Green and yellow characters cause eyes fatigue lighter than red and blue characters [3]. Green characters cause eyes fatigue smaller than white characters. Besides color, brightness, contrast, and matching of background color, target color also make a different effect to eyes [3].

This paper focused on how different materials affect the cockpit's visual performance in direct sunlight.

II. ARTIFICIAL NEURAL NETWORK

Artificial Neural Networks (ANNs) are called Neural Networks (NNs) or Connectionist Model in short [4, 5]. They're a kind of algorithm mathematical model which can simulate animals' behavior characteristics of neural networks and conduct distributed parallel information processing. These networks rely on the complexity of system by adjusting the relationship of the large internal mutual connections of nodes, to process information. Artificial Neural Networks have the capacity of self-learning and self-adaption. Providing a batch of mutual correspondence input/output data in advance, ANNs can analyze the potential law and calculate output with the final new input data according to these laws. These study and analysis process are called 'training'. Characteristics and superiority of ANNs are reflected in three aspects: Firstly, ANNs have function of self-learning. Secondly, ANNs have function of association and storage. Thirdly, ANNs have ability of seeking for optimal solution with high speed. Therefore, ANNs are widely used in medical, automatic control etc, and have important application in dealing with combinatorial optimization problem, pattern recognition and image processing [6].

Self-organization Kohonen network and multilayer perceptron BP network are two artificial neural networks commonly used. The former is mainly used for pattern

analysis and pattern recognition. The latter is mainly used to approximate complex non-linear relationship of input and output [7][8].

III. Database Profile And Research Direction

As shown in Figure 1, the database is composed by 750 independent data. Each data has information of 12 dimensions beside material ID as shown in Table I.

In the database, obviously, color temperature of light source is 6000K. Transmissivity of each material is zero (light-proof material). The sum of reflectivity and absorptivity is 100. Therefore, these 3 columns are invalid data which could be rejected. Two relations have been summarized following with reminding data of 9 dimensions.

$$[brightness,\ luminous\ intensity] = f[material\ \ properties,\ light\ \ source\ \ properties] \quad (1)$$

$$[contrast,\ color\ \ coordinate] = g[material\ \ properties] \quad (2)$$

p.s. The left sides of formula (1) and (2) are output information, while the right sides are input information, as well as symbols of function.

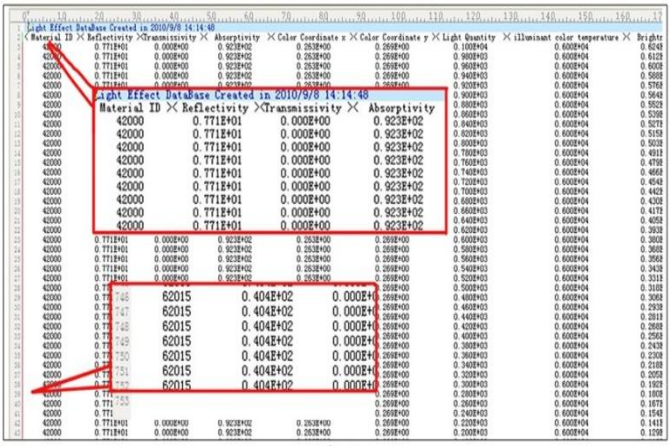

Figure 1. Database Scheme

TABLE I.

Input Information				Output Information	
Material properties		Illuminant properties			
Column Number	***Name***	***Column Number***	***Name***	***Column Number***	***Name***
1	Reflectivity	6	Luminous flux	8	Brightness
2	Transmissivity	7	Illuminant Color Temperature	9	Luminous Intensity
3	Absorptivity			10	Contrast
4	Material Coordinate x			11	Color Coordinate x
5	Material Coordinate y			12	Color Coordinate y

Due to the formula (2), contrast and color coordinates of output only relate to material properties (reflectivity, color coordinate x, color coordinate y). After contrast and coordinates of output analyzed, materials with draw near properties are chosen for the purpose of further screening. SOM network fits this part of job.

After material finalized, the value of brightness and luminous intensity could be obtained based on approximate input/output relationship by BP network. Thus, the optimal light source condition would be determined. This part of job is completed by BP network.

IV. Simulation Results

A. Summary of research results based on SOM network

Contrast and color coordinates only rely on material. Total 15 groups of three dimensional data involving contrast and color coordinates are sampled from 15 kinds of materials accordingly. The distribution of sample points is shown in Figure 2(a).

As shown in Figure 2(a), almost all sample points are ranked in a straight line because each degree of freedom has different scale. This sample will bring adverse impact for SOM network which needs standardization. Standardization uses a square affine transformation with a vertex as original point. Sample points after standardization are shown in Figure 2(b).

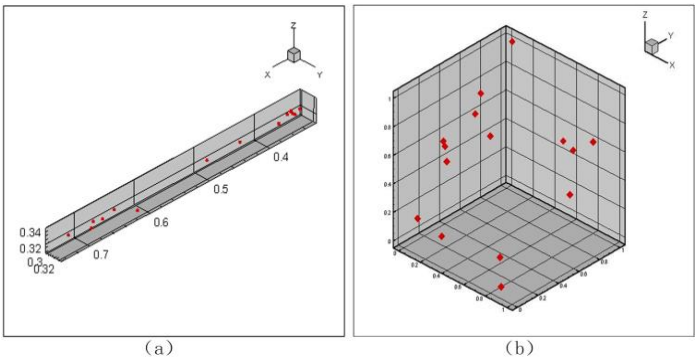

Figure 2. Distribution of sample points: (a) original distribution of sample points and (b) distribution of sample points after transformation

Initialization parameters of SOM network are shown in Table II. After initializing, parameters of the training process of SOM network have various alternatives. After trying, training results perform well when parameters are set according to Table III.

After training, error curve is plotted and shown in Figure 3, indicating that the error will be less than 10e-4 after 5500 steps. When the training of neural network is completed, response of each neuron is obtained according to every input pattern. Respond surfaces of all samples are shown in Figure 4(a).

TABLE II.

Topological Structure	Dimension of SOM network	Function Type of Epsilon Neighborhood	Initializing Pattern
Rect	10*10	Gaussian	random

TABLE III.

	Training Times	Changing Rule of Learning Rate	Initial Learning Rate	Initial Superior radius of neighbourhood
1	501	Linear	0.1	10
2	5001	Inverse	0.03	3

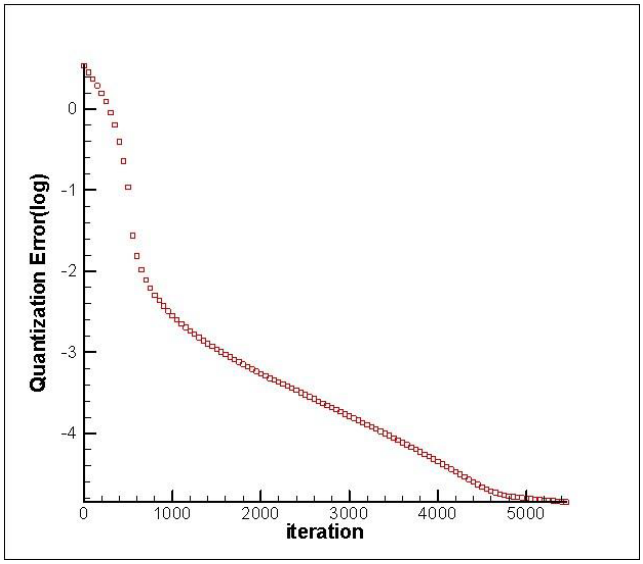

Figure 3. Error curve

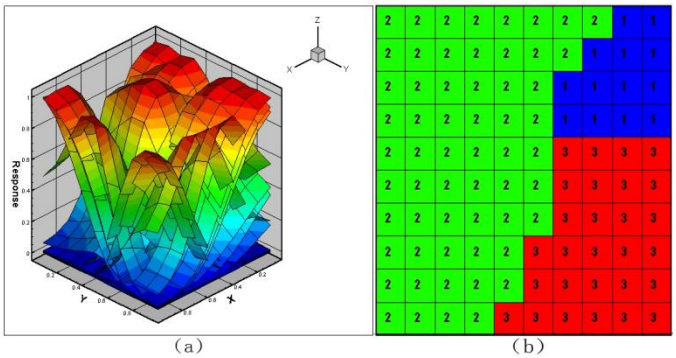

Figure 4. (a) respond surfaces and (b) mapping

All of 15 input samples are divided into groups in according to the above respond surfaces, as shown in Table IV. Samples divided into the same group can active neurons in the same district, which can produce maximum responses. Thus, a 2-dimension mapping is shown in Figure 4(b). What is shown in Figure 5 are 2-dimension response diagrams of representative samples of above 3 groups. Scattered sample points are divided into 3 groups by certain rules in Figure 6.

TABLE IV.

Number	Sample Number						
1	1	3					
2	2	4	5	6	8	10	12
3	7	9	11	13			

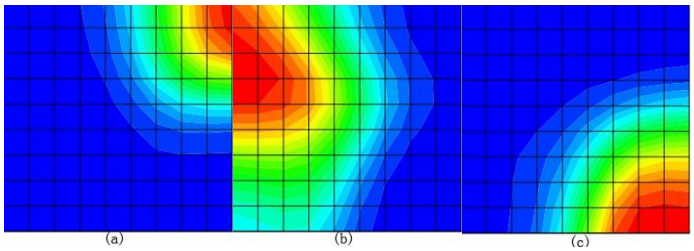

Figure 5. 2d response diagram

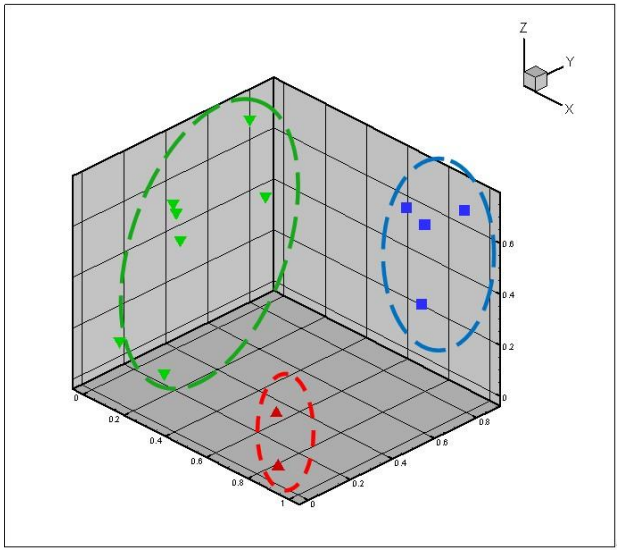

Figure 6. Scattered sample points

B. *Summary of simulation results based on BP network*

After superfluous data are ruled out, data of 9 dimensions remain, while 4 dimensions are used for input and other 5 dimensions are output. And qualitative mapping relations are got and shown as follow:

1) If luminous flux is set 1000lm and illuminant color temperature is set 6000K, brightness, luminous intensity, contrast, color x and color y are the function of material absorption, color coordinate x and color coordinate y.

2) If material properties are given and illuminant color temperature is set 6000K as well, brightness and luminous intensity are monodrome function of luminous flux.

Constrain condition: Material transmissivity is 0. Luminous flux is 1000lm. Illuminant color temperature is 6000K.

Establish the corresponding relationship between material absorption, color coordinate x, color coordinate y, and color x, color y by Matlab neural network toolbox. Total samples are 15. 12 of them are training samples, while the others are testing samples. BP network adopts 3-layer structure, 4 input neuron, 2 output neuron and 2000 training steps. After training, the error salvage value curve is shown in Figure 7. The training sample and testing sample are shown in Figure 8(a) and Figure 8(b). The main error of testing sample is -0.19%.

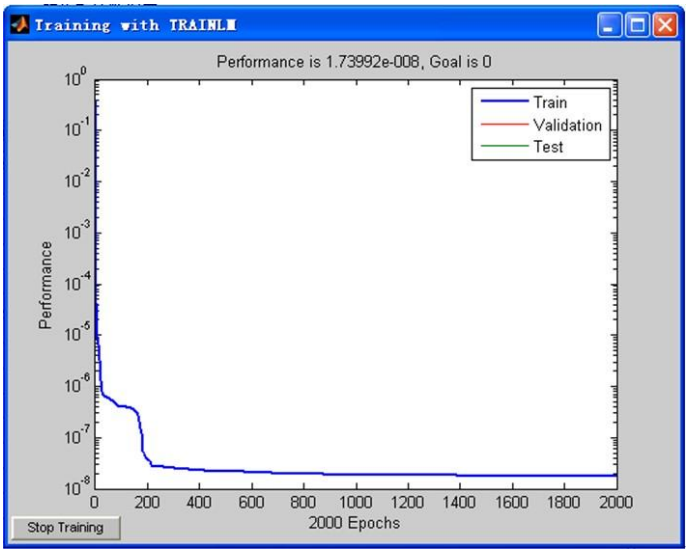

Figure 7. Error salvage value curve

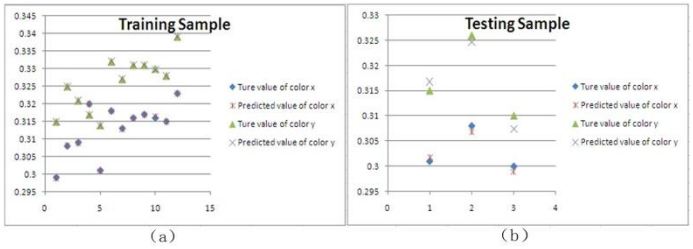

Figure 8. (a) Training Sample and (b) Testing Sample

Establish the corresponding relationship between absorption, color coordinate x, color coordinate y, and contrast. Then the training results of color x and color y are shown in Table V, as well as training results of contrast in Table VI. Although average error is 0.01%, maximum error is about 5%. The main reasons are the number of samples is relatively a little fewer and the corresponding relationship is uncertain, which will be investigated further. The corresponding relationship between material absorption, color coordinate x, color coordinate y, and brightness, luminous intensity is obtained through Matlab neural network. The result doesn't perform well, which needs further study.

If material properties are given and illuminant color temperature is set 6000K as well, brightness and luminous intensity are almost direct proportional to luminous flux. The following figures are data researches of two materials. Approximating by a linear function with intercept of zero, square of linearity R is 0.9997, which is in the range of allowable error. The relationship of brightness and luminous intensity of different material is shown in (a)-(d) of Figure 9.

Obviously, brightness is liner with luminous intensity. Without building neural network, brightness and luminous intensity of random luminous flux can be calculated according to brightness and luminous intensity of different material with 1000lm aforementioned.

TABLE V.

Color x	Color y	Training Results of Color x	Training Results of Color y	Error x	Error y
0.301	0.315	0.302	0.317	0.27%	0.57%
0.308	0.326	0.307	0.325	-0.39%	-0.43%
0.3	0.31	0.299	0.308	-0.37%	-0.81%
0.299	0.315	0.299	0.315	-0.03%	0.00%
0.308	0.325	0.308	0.325	0.06%	-0.03%
0.309	0.321	0.309	0.321	-0.03%	0.00%
0.32	0.317	0.320	0.317	0.00%	0.00%
0.301	0.314	0.301	0.314	0.00%	0.00%
0.318	0.332	0.318	0.332	-0.03%	0.03%
0.313	0.327	0.313	0.327	-0.06%	0.03%
0.316	0.331	0.316	0.331	-0.06%	0.03%
0.317	0.331	0.317	0.331	-0.03%	0.03%
0.316	0.33	0.316	0.330	0.13%	-0.06%
0.315	0.328	0.315	0.328	0.00%	0.00%
0.323	0.339	0.323	0.339	0.00%	0.00%

TABLE VI.

Contrast	Training Results of Contrast	Error
0.6554	0.625	-4.64%
0.3478	0.345	-0.81%
0.6731	0.7077	5.14%
0.4792	0.4791	-0.02%
0.3543	0.3718	4.94%
0.3422	0.3435	0.38%
0.6162	0.6167	0.08%
0.3615	0.3498	-3.24%
0.7294	0.7256	-0.52%
0.4378	0.4295	-1.90%
0.6515	0.6515	0.00%
0.3416	0.3416	0.00%
0.6861	0.6907	0.67%
0.3522	0.3522	0.00%
0.3633	0.3633	0.00%

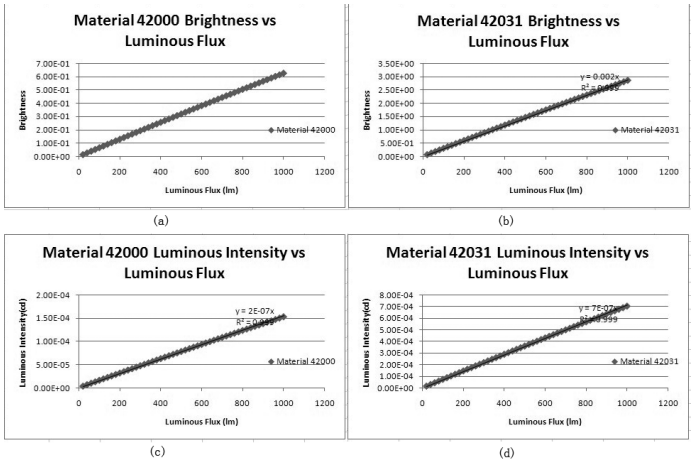

Figure 9.

V. CONCLUSIONS

This paper present a system used for multivariable coupling by ANNs method. The method proves to be usefull and effective. SOM network is used for selecting different materials variables while BP network is used for non-linear fit. Approximate relationship between material variables and photometric variables established, so that there's corresponding output for arbitrary input within the approximate relationship. In this way, large amount of data would be obtained without experiment.

In this paper, although the case has 9 dimensions, it can also be applied into more dimensions. The degree of accuracy is depended on the scale of database.

ACKNOWLEDGMENT

The work is sponsored by National Basic Research Program ("973" Program) of China, Issue Number 2010CB734106.

REFERENCES

[1] J. B. Ding. "Synthetic Fuzzy Evaluation of the Quality of Light Conditions of the Human2Machine System", Journal of Xuzhou Institute of Architectureal Technology, 2(2), 11-18 (2002).

[2] L. Z. Ge and F. P. Hu, "The Ergonomics Study on Multi-element Visual Display" Journal of Developments in psychology, 9(3), 201-204 (2001).

[3] D. Q. Zhang, Z. J. Zhang and H. Z. Yang, "VDT interface color vision work efficiency: Tonal factors on the visual performance impact," Psychological Science, 31(2), 328-331 (2008).

[4] Liqun Han. "Artificial neural network course. Beijing University of Posts and Telecommunications Press, (2006).

[5] M. Hagan. Neural Network Design. China Machine Press, (2002).

[6] M. A. L. Nicolelis and S. Ribeiro "Seeking the neural code", Scientific American, 295(6), 70-77 (2006).

[7] T. Kohonen, "The Self-Organizing Map", IEEE, 78(9), 1464-1484, (1990).

[8] X. Wen, chap. 10 in Matlab neural network simulation and application, pp. 250-300, Science Press, Beijing (2003).

The Fault Location Method Research of Three-Layer Network System

Hu Shaolin[1,2], Li ye[2], Karl Meinke[3]
(1. State Key Laboratory of Astronautics, Xi'an, P.O. Box 505-16, 710043,China)
(2. Automation School, Xi'an University of Technology, Xi'an, 230027)
(3. Royal Technical Institute of Sweden, Stochastic, Sweden)

***Abstract*— The fault location technology research of three-layer network system structure dynamic has important theoretic value and apparent engineering application value on exploring the fault detection and localization of the complex structure dynamic system. In this article, the method of failure propagation and adverse inference are adopted, the fault location algorithm of the three-layer structure dynamic network system is established on the basis of the concept of association matrix and the calculating method are proposed, and the simulation calculation confirmed the reliability of this paper. The results of the research can be used for the fault diagnosis of the hierarchical control system、testing of the engineering software and the analysis of the failure effects of layered network of all kinds and other different fields.**

Keywords- Three-layer network; fault propagation; fault location.

I. INTRODUCTION

Nearly half a century, the automation technology of system during operating process has developed along two general directions as a whole. One is the optimization and intelligent of the system in normal conditions, the other is fault monitoring and safety of the system in failure. Especially the latter, since the 1970s, Berd put forward a control system which is based on the analytic redundant fault detection and diagnosis, it was widely valued by the international and domestic academic industry and the engineering application industry, successively proposed and developed a series of fault detection and diagnosis

methods that are novel and practical（FDD：Fault Detection and Diagnosis）, such as FDD method based on signal processing、FDD method based on data-driven、FDD method based on structural redundancy、FDD method based on information redundancy、method based on equivalent space and FDD method based on system simulation etc. The concerns of the research have developed from early static equipment or the single fault of the system to the concurrent malfunction of the complex structure system and the continual failure of the system during running process.

For the fault monitoring and security of a complicated structure dynamic system, it has been the focus and difficulty that how to use the anomaly information monitored by all sorts of sensing/sensors or other measuring equipment to fault location accurately.

Complex structure dynamic system has a complex relationship between relevant components, the difficulty of the fault location become higher and higher, in order to overcome the technology difficulty of the develop of the fault diagnosis expert system and the technical problems of familiar reasoning process conflicts which are based on rule reasoning or cases, this paper develops a practical and concise fault location algorithm based on mathematical operation, which can locate the fault point fastly, it also solves the difficult problems of fault location of the complex structure system and proves the effectiveness of the new method through the simulation results.

II. THE STATUS ANALYSIS OF COMPLEX STRUCTURE SYSTEM AND CAUSAL MODELING

Any complex structure dynamic system is usually composed of several functional subsystem, each subsystem includes several components. Similarly, each subsystem can also be further broken down into some functional subsystem in level 2 and each subsystem in level 2 also includes several small parts.

Whether the systems or the subsystems or the components, only when it transfer information to the outside system directly or indirectly, can we perceive or judge whether it runs normal or not. In other words, whether the state of work is normal or not is unknown to the outside world without any way to transform subsystems or components to the outside system directly or indirectly. For this kind of system that cannot transfer parts of information or subsystems to the outside system, we call it a "black hole".

For this kind of system, when malfunction happened, how to locate fault source becomes difficult, considering the complexity of the system, causal modeling method is adopted in this paper, namely layered network modeling method, it sets up the correlation matrix through the top and the bottom of the association. So, the changes of the bottom can find the changes of the top source through the incidence matrix.

III. THE DESIGN AND CALCULATION OF THE TOP - BOTTOM RELATING MATRIX

For the three layer network in figure 1, simple to set the top nodes as $V_1 = \{v_{1,i} \mid i = 1,2,\cdots,n_1\}$, to set the middle nodes as $V_2 = \{v_{2,i} \mid i = 1,2,\cdots,n_2\}$,to set the bottom nodes as $V_3 = \{v_{3,i} \mid i = 1,2,\cdots,n_3\}$,

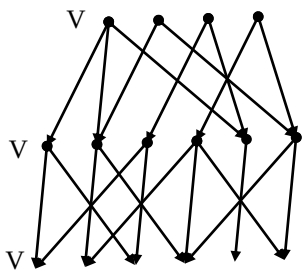

Figure 1. The structure schematic drawing of three layer network

For the bottom nodes $v_{1,j} \in V_1$, defining status symbol values for nodes

$$d_1(v_{1,j}) = \begin{cases} 1, node\ v_{1,j}\ is\ fault \\ 0, node\ v_{1,j}\ is\ normal \end{cases} \quad (1)$$

And the joint strength between adjacent layer contacts nodes $v_{s,i} \in V_s$ and $v_{s+1,j} \in V_{s+1}$

$$b(v_{s,t}, v_{s+1,j}) = \begin{cases} 1, & v_{s,j}\ and\ v_{s+1,j}\ has \\ & edge-juction \\ 0, & v_{s,j}\ and\ v_{s+1,j}\ has \\ & not\ \ edge-juction \end{cases} \quad (s=1,2) \quad (2)$$

Thus, using operator "and" $\wedge$ and operator "or" $\vee$ of Borel algebra, we can calculate the flag values of the middle layer nodes $v_{2,j} \in V_2$ by the next formula

$$d_2(v_{2,j}) = \bigvee_{t=1}^{n1} \{ d_1(v_{1,t}) \wedge b(v_{1,t}, v_{2,j}) \} \quad (3)$$

Similarly, defining the flag values of the bottom nodes $v_{3,j} \in V_3$

$$d_3(v_{3,j}) = \bigvee_{t=1}^{n2} \{ d_2(v_{2,t}) \wedge b(v_{2,t}, v_{3,j}) \} \quad (4)$$

Proposition 1: if $d_2(v_{2,j}) = 0$, so either every top layer node does not broke down or the node which brokes down does not spread into the middle layer node $v_{2,j} \in V_2$, conversely, if $d_2(v_{2,j}) = 1$, so the top layer has at least one node broke down, and the failure influence spread into the middle layer nodes $v_{2,j} \in V_2$.

Proof. By formula (4) and the operation rule of Borel operator, if $d_2(v_{2,j}) = 0$, so for all the top layer nodes $v_{1,t} \in V_1$, we can have $d_1(v_{1,t}) = 0$ or $b(v_{1,t}, v_{2,j}) = 0$, it means that either this node does not broke down or there is no united way between this node and the middle layer node.

If $d_2(v_{2,j}) = 1$, so there must be $1 \le t_0 \le n_1$ to make $d_1(v_{1,t_0}) \wedge b(v_{1,t_0}, v_{2,j}) = 1$,

it means $d_1(v_{1,t_0}) = 1$ and $b(v_{1,t_0}, v_{2,j}) = 1$.

Thus, the top layer node v_{1,t_0} has broken down and its fault can transfer to middle node $v_{2,j}$ by the path $(v_{1,t_0}, v_{2,j})$.

Proposition 2: if $d_3(v_{3,j}) = 0$, so the middle layer node either works properly or the influence of the abnormal node do not transfer to the bottom layer node $v_{3,j} \in V_3$, reversely, if $d_3(v_{3,j}) = 1$, so there is at least one top middle node is abnormal and its fault influence transfer to the bottom layer node $v_{3,j} \in V_3$.

Proof. It is familiar with proposition 1, so omit the proof process here. Making flag vector

$$\vec{d}_1 = (d_1(v_{1,1}), \cdots, d_1(v_{1,n1})),$$

setting the first k component of vector to 1, the rest is 0 respectively.

$$\vec{d}_1{}^k = (1, \cdots, 1, \cdots, 0) \quad (5)$$
$$\uparrow$$
$$the\ first\ k\ component$$

Using the flag value of the middle layer node $d_2^k(v_{2,j})$ $(j = 1, \cdots, n_2)$ can calculate the numbers of the propagation paths that the top layer node uses to transfer the fault to the bottom layer node.

$$s_i(k) = \sum_{j=1}^{n2} d_2^k(v_{2,j}) \wedge b(v_{2,j}, v_{3,i}) \quad (6)$$

According to the definition of the formula (6) and the proving process of propoistion1 and proposition 2, we can easily derive the next conclusion:

Theorem 1: if $s_i(k) = t$, showing that the top layer node $v_{1,k}$ is broken down and it will transfer its fault to the bottom layer node $v_{3,i}$ through t different paths.

If $s_i(k) = 0$, it shows that the fault of the top layer node $v_{1,k}$ do not effect the bottom layer node $v_{3,i}$.

Proof: according to formular (6) and the operational rule of Borel operator, we can find that if $d_2^k(v_{2,j}) \wedge b(v_{2,j}, v_{3,i}) = 1$, it means $d_2^k(v_{2,j}) = 1$ and $b(v_{2,j}, v_{3,i}) = 1$. Thus, the top layer node $v_{1,k}$ is borken down and it can transfer its fault from the

middle layer node $v_{2,j}$ to the bottom layer node $v_{3,i}$ by the path $(v_{2,j}, v_{3,i})$.

Thus, the formula (6) shows the numbers of paths that top layer node uses to transfer its fault form different middle layer nodes to the bottom layer nodes.

Obviously, if

$$\sum_{i=1}^{n_3} s_i(k) = 0, \text{ So, } s_1(k) = \cdots = s_{n3}(k) = 0.$$

According to the proposition 3, the fault of the first k layer node can not be transferred and can not effect the bottom layer node. We called these top layer nodes isolated points.

For the three-layer network system without isolated points, we can eastablish a top-bottom associated matrix by calculating the numbers of the paths $s_i(k)$ that the top layer node uses to transfer its fault to the bottom layer nodes.

$$M_{1-3} = \begin{matrix} v_{3,1} & \cdots & v_{3,n3} \\ \end{matrix} \begin{pmatrix} f_{1,1} & \cdots & f_{1,n3} \\ \vdots & & \vdots \\ f_{n1,1} & \cdots & f_{n1,n3} \end{pmatrix} \begin{matrix} v_{1,1} \\ \vdots \\ v_{1,n1} \end{matrix} \quad (7)$$

In the formula (6)

$$f_{k,i} = s_i(k) \Big/ \sum_{i=1}^{n3} s_i(k) \quad (k = 1,\cdots,n_1; i = 1,\cdots,n_3).$$

Obviously, the matrix M_{1-3} has the next qualities:

(1) $0 \le f_{k,i} \le 1$ $(k = 1,\cdots,n_1; i = 1,\cdots,n_3)$, it means every elements of the associated matrix is a nonnegative number that is not exceeding 1.

(2) $\sum_{j=1}^{n_3} f_{k,i} = 1$ $(k = 1,\cdots,n_1)$, it means that all elements in each row of the matrix added to 1 .

IV. The Algorrthm Of The Fault Location

Bringing all different groups of the formular (5) into the formular (3) to calculate the flag value $d_2^k(v_{2,j})$ $(j = 1,\cdots,n_2)$ using proposition 1 and proposition 2, then bringing the flag value $d_2^k(v_{2,j})$

into the formular (4), after the above process, we can calculate the state flag matrix:

$$B_{1-3} = \begin{matrix} \vdots v_{3,1} & \cdots\cdots & v_{3,n3} \\ \end{matrix} \begin{pmatrix} d_3^1(v_{3,1}) & \cdots & d_3^1(v_{3,n3}) \\ \vdots & & \vdots \\ d_3^{n1}(v_{3,1}) & \cdots & d_3^{n1}(v_{3,n3}) \end{pmatrix} \begin{matrix} v_{1,1} \\ \vdots \\ v_{1,n1} \end{matrix} \quad (8)$$

Obviously, the flag value $d_3^i(v_{3,j})$ of i-th $(i = 1,2,\cdots,n_1)$ row and the j-th $(j = 1,2,\cdots,n_3)$ in the state flag matrix B_{1-3} reflect whether the top layer node $v_{1,i}$ can transfer its fault to the bottom layer node $v_{3,j}$, reversely, $d_3^i(v_{3,j}) = 0$,shows that the bottom layer node $v_{3,j}$ would not be effected by the top layer node $v_{1,i}$.

According to the analysis above, we can establish the fault location algorithm: we supposed that every bottom layer node is installed with a sensor, so we can achieve the fault omen information of the layer node directly. According to the state information of the bottom layer of the system, we can demarcate the state of the bottom layer nodes

$$f_3(v_{3,j}) = \begin{cases} 1, \textit{node } v_{3,j} \textit{ has fault omen} \\ 0, \textit{node } v_{3,j} \textit{ is normal} \end{cases} \quad (9)$$

Calculating the weighting indicator:

$$g_i = \sum_{j=1}^{n_3} f_{i,j} \left\{ d_3^i(v_{3,j}) \wedge f_3(v_{3,j}) \right\} \ (i = 1,2,\cdots,n_1) \quad (10)$$

It is easy to prove $0 \le g_i \le 1$ $(i = 1,2,\cdots,n_1)$. When $g_i = 1$, we can diagnose the top layer node $v_{1,i}$ is the source of the fault, when $g_i < 1$, we can diagnose the top layer node $v_{1,i}$ is normal (or the fault omens of the bottom layer nodes are not caused by the top layer node $v_{1,i}$).

In practical operation, considering the fault omen or the sensitivity of the detection sensor, when $g_i \approx 1$ and $g_i << 1$, we can make the similar judge as above.

V. Simulation Calculation

For the three-layer network as the figure 1 shows, we use 4×4 matrix

$$D1 = \begin{bmatrix} 1 & 0 & 0 & 0 \\ 0 & 1 & 0 & 0 \\ 0 & 0 & 1 & 0 \\ 0 & 0 & 0 & 1 \end{bmatrix}$$

to express all the groups of the formula (5), comparing the matrix D1, we assume the fault nodes are $v_{1,1}$ and $v_{1,3}$, according to the figure 1, we can calculate the flag matrix of the bottom layer

$$f = [1 \quad 0 \quad 1 \quad 0 \quad 1 \quad 0].$$

Then, calculating the state flag matrix when the top layer nodes transfer its faults to the bottom layer nodes by the formulae (3) and (4)

$$D3 = \begin{bmatrix} 1 & 1 & 1 & 1 \\ 0 & 1 & 0 & 1 \\ 1 & 0 & 1 & 0 \\ 0 & 1 & 0 & 1 \end{bmatrix},$$

using $f_{k,i} = \dfrac{s_i(k)}{\sum_{i=1}^{n3} s_i(k)} \quad (k = 1, \cdots, n_1; i = 1, \cdots, n_3)$ to help us to get the weighting matrix, it is also the top-bottom associated matrix

$$F = \begin{bmatrix} 0.2 & 0.2 & 0.2 & 0.2 \\ 0 & 0.3333 & 0 & 0.3333 \\ 0.3333 & 0 & 0.3333 & 0 \\ 0 & 0.25 & 0 & 0.25 \end{bmatrix},$$

finally, we can get the weighting indicator matrix of the top layer nodes by using the formula (10)

$$g = [0.6 \quad 0 \quad 1 \quad 0]$$

. We can make the conclusion from the simulation result of matlab that g(1,1) and g(1,3) satisfy the condition $g_i \approx 1$,so we can judge the nodes $v_{1,1}$ and $v_{1,3}$ are the fault nodes, it proves the accuracy of the algorithm.

ACKNOWLEDGMENT

The authors wish to express special thank to the financial support of the National Natural Science Foundation of China, Grant No. 61074077.

VI. CONCLUSION

It is necessary to detect and protect the state of the complex structure system in the engineering field, how to detect and repair timely when faults happen to the complex structure system is more important. For the complex system which concludes many different functional subsystems, how to locate the source of the faults quickly is the key point of this paper. The paper set a example as the three-layer network, putting forward a new algorithm of fault location that can locate the source of fault by the detection of sensors to the bottom layer nodes, it can save much time for the next work. In the last of the article, we make a simulation test to the algorithm using the software matlab, the result prove the accuracy of the algorithm. Also, the algorithm is only tested in the three-layer network system, but we cannot get the accuracy result for the more complex system and it will be the main direction of the research in the future.

Reference

[1] Zhang Yingwei，S.Joe Qin. The Fault Diagnosis of the Complex Industry Process [in chinese]. Journal of Northeast University Press, Shenyang, 2008

[2] Zhou Donghua， Sun Youxian. Fault Detection and Diagnosis Techonlogy of the Control System [in chinese]. Tsinghua University Press, Beijing,1994

[3] Lijing，Liu Hongwei，Dongjian，Shu Yanjun. The Cluster Fault Management System Structure Based On the Independent Calculation [in chinese]. Journal of Tsinghua University，2011，S1:1—5

[4] Heidtmann, F. Soffker, D. Virtual Sensors for Diagosis and Prognosis Purposes in the Context of Elastic Mechanical Structures. Sensors Journal, IEEE,2009,9(11):1577-1588

[5] Lira, D.N. Garcia, J.l. Junqueira, F. Miyagi, P.E. Fault detection in Flexible Assembly Systems using Petri net. Latin America Transaction, IEEE, 2008,6(7):572-578

[6] Xiong Hao, Sun Cai-xin: Arificial Immune Network Classification Algorithm for Fault Diagonsis of Power Transformei. Power Delivery, IEEE Transactions, 2007, 22(2):(930-935)

[7] Dorel Arordachioaie, Emil Ceangaa, et al. Detection and classification of non-linearities based on Volterra kernels processing. Engineering Applications of Artificial Intelligence,The International Journal of Intelligent Real-Time Automation,2001,14(4): 497-503

[8] Xue Dingyu: The Simulation Technology and Application of the System Based on Matlab/Simulink [in chinese].Tsinghua University Press, Beijing, 2011